 doi:10.20944/preprints201806.0466.v1

Analysis of the Spatial and Temporal Distribution of the 2011 Earthquakes in Lake Van Area and Rupture Complexity of the Aftershock Sequence in Eastern Anatolia, Turkey

Mustafa Toker: 1. University of Oulu, Sodankylä Geophysical Observatory, Laboratory of Applied Seismology, POB 3000, FIN-90014, Oulu/Finland

2. Yuzuncu Yıl University, Department of Geophysical Engineering, Zeve Campus, 65080, Van/Turkey, tokermu@gmail.com

Corresponding Author:
Dr. Mustafa Toker
Yüzüncü Yıl University, Department of Geophysical Engineering, Zeve Campus, Van, Turkey
Phone: +90-(0) 543-624-7503
Fax: +90-(0) 422-273-3756
E-mail: tokermu@gmail.com

© 2018 by the author(s). Distributed under a Creative Commons CC BY license.

Abstract

This study presents an analysis of the spatial and temporal distribution of the two large destructive earthquakes that occurred in Lake Van area on October 23, and November 9, 2011, together with the azimuth-dependent distribution of the seismic activity and microseismicity clusters after the mainshocks, associated with the complex rupture processes of their aftershock sequence. The sequence began with the magnitude Mw 7.1 earthquake of 23 October and a second destructive earthquake of Mw 5.6. The aftershock sequences of the two mainshocks were linked to the local crustal faults beneath Lake Van area, followed successively and produced unusually intense activity and significant damage in the area. The main purposes of this study are to document the spatial and temporal distribution and evolution of the October 23, 2011 aftershock hypocenters and the azimuth-dependent distribution of seismic activity, and to understand the spatial and temporal character of the aftershock sequence using the distributional and evolutional patterns of the aftershock hypocenters. A total of 10,000 aftershocks were obtained from seismic data with a high signal-to-noise ratio over collected over three years from October 23, 2011 to March 2014. These aftershocks were plotted for the time periods from November 2011 through March 2012 to March 2014 and ≈ 5000 aftershocks were retained in the depth versus distance cross-sections to detect the clusters in the first step of study (November 2011-March 2012). The focal depth distribution of the aftershock clusters, the migration of hypocenter activity and microseismicity clusters were analyzed and the distributional patterns of the detected clusters were assessed using the geometric distribution of the aftershock hypocenters. The spatial and temporal distribution of aftershocks reveal interesting key features of the deep rupture complexity of the Van earthquake: (1) most prominent aftershocks have been located in the upper crust at depths shallower than 10 km beneath ruptured area, indicating that

Preprints (www.preprints.org) | NOT PEER-REVIEWED | Posted: 28 June 2018 doi:10.20944/preprints201806.0466.v1

the upper crust is brittle and seismogenic; (2) two spatial clusters have been detected at 8-10 km depths and the upward extrapolation of these clusters intersects with faults; the main cluster (60 km wide) bounded by inferred reverse faults (f3 and f4) and the central cluster (25-30 km wide) bounded by faults (f1 and f2); (3) these spatial clusters form the largest volumetric pattern of the conical-shaped cluster at depths of about 25-30 km of the azimuth-dependent rotational projections, suggesting azimuthal distributions of deep rupture characteristics; and (4) the strongest temporal cluster of microseismicity derived from temporal distribution of aftershocks has been detected within an area of about 2.5-3.0 km^2 and it is spatially observed at 20 km depth within the central cluster, suggesting progressive failure of the adjacent patches of possible fault.

Keywords: Lake Van, Van earthquake, aftershock hypocenters, rupture complexity, azimuthal distribution, aftershock clusters, microseismicity

Preprints (www.preprints.org) | NOT PEER-REVIEWED | Posted: 28 June 2018 doi:10.20944/preprints201806.0466.v1

1. Introduction

During the last ten years, seismological observations of aftershock seismicity from the interplate and intraplate seismotectonic settings and magnitudes have indicated that variations in stress state less than 1 bar are able to induce the reactivation of nearby faults that are close to failure, either as long-term post-seismic deformation (e.g., spatial and temporal occurrence of aftershock activity) or as secondary larger earthquakes (e.g., compound seismicity). This phenomenon has been described as a triggering process (King et al. 1994; Harris et al. 1995; Benito et al. 2004). The triggering process may involve the anomalous generation of aftershocks or secondary mainshocks with different focal mechanisms, with prominent changes in the spatial and temporal character of the mainshock aftershock sequence in a given focal area which increases or decreases for several months or years after a mainshock (Stein and Lisowski 1983; Reasenberg and Simpson 1992; Stein 1999; Benito et al. 2004).

Lake Van located in the province of Van in eastern Anatolia is characterized by intraplate seismicity and highly active compressional shear strains (Kutoğlu et al. 2016) with long-term aftershocks of magnitudes more than 3.5-4.0 occurring repeatedly (Toker 2013; 2014) (Figure 1). Toker (2014; 2015) has shown that these aftershock events in the temporal form of multi-clusteral patterns are repeating ruptures of asperities comprising areas of large coseismic slip, which are locked during interseismic period. On October 23, 2011, a great thrust earthquake of magnitude Mw 7.1 occurred in the Lake Van area (Irmak et al. 2012; Bayrak et al. 2013; Elliott et al. 2013; Moro et al. 2014; Toker 2015) (Figure 1). The earthquake and its strong aftershocks activated the ~ 27-km-long Blind Thrust fault system that marks the accretionary wedge complex and the transition between the basins of Lake Van and Lake Erçek (Figure 1) (Doğan and

Karakaş 2013; Karakaş et al. 2013; Elliott et al. 2013; Doğan et al. 2014). The multi-crustal occurrence and distribution of long-period aftershock activity and focal mechanism of this larger event show a northeast–southwest striking rupture plane dipping towards the northwest (Irmak et al. 2012; Toker 2013; Utkucu et al. 2013; Fielding et al. 2013; Bayrak et al. 2013) (Figure 2). The rupture gradually expanded near the hypocenter and was shaped in a sigmoidal-like propagation (Figure 2). It is thought that the earthquake occurred as a result of a long-term high plateau uplift (Görür et al. 2015) and an eastward oblique tectonic extrusion of the Lake Van basin (Toker and Şengör 2011; Toker and Ecevitoğlu 2012a, b).

The October 23, 2011 Van earthquake was a somewhat unusual case concerning the anomalous occurrence and the spatial and temporal distribution of its aftershocks ($M \geq 4.0$) in Lake Van (Figures 2 and 3). The Van earthquake was followed by numerous aftershocks with the same origin and most of the aftershock activity was restricted to a narrow area, bounded by the faults of the lake (Figures 1 and 2); ~2,828 events occurred in the first month (November 2011), and 4,853 in the first five months (November 2011- March 2012), nearly half of which were larger than Mw 2.5-3.0 (Figure 3b). Until the end of 13 April 2012 over a period of 163 days, the total activity of 5,304 aftershocks comprised of 184 Mw $\geq$ 4.0 and 13 Mw $\geq$ 5.0 events (Bayrak et al. 2013; Toker 2014). This earthquake was associated with the local fault system aligned with the Lake Van basin that extends from west to east (Figures 1 and 2) (Moro et al. 2014). Two weeks later, on 9 November, a second major earthquake of Mw 5.6, the Edremit event (5-7 km depths), occurred the near the southeastern coast of Lake Van along the north dipping a normal oblique-strike-slip Edremit fault (Utkucu 2013; Utkucu et al. 2013; Doğan et al. 2014) (Figure 2). This second earthquake was also associated with the local fault system (Ketin 1977; Utkucu 2006). Both the epicenter location and the fault focal solution of the Edremit event obviously indicate that it occurred on a different fault (Figure 2). The aftershock sequence of the November 9, 2011 Edremit earthquake worsened the situation in the area that had been affected by the previous Van earthquake. The epicenter locations and the fault focal solutions of these earthquakes indicate that they occurred on different fault systems (Figure 2).

The two mainshocks of October 23 and November 9, together with thousands of events of lesser magnitude and their respective aftershock sequences, produced an intense period of intraplate seismic activity over a short time interval. This seismic activity did not appear to decrease over time and frequency, according to the known laws. The temporal propagation and evolution of the Van aftershock sequence showed a complex short and long term dynamic evolution in the aftershock area (Toker 2013; 2014; 2015). This is repeated for all the events, and may have induced alternating stress increases and decreases in either time or space, thus generating the observed clusters, declusters and dynamic complexity in the aftershock sequence (Toker 2015). If this is the case, the rupture area of the Van mainshock ruptures repeatedly in the consecutive aftershocks and it is extremely important to reveal aftershock hypocenters of the mainshock in order to understand the focal depth nature of the rupture complexity. This suggests that the present probability of the repeated aftershock occurrence ($Mw \geq 4.0$-4.5) in the mainshock area is quite high.

Soon after the Van earthquake, many geologists undertook field investigations of the surface ruptures and co-seismic deformation (Irmak et al. 2012; Koçyiğit 2012; Doğan and Karakaş 2013; Karakaş et al. 2013; Doğan et al. 2014). However, because of the occurrence of seismic-related surface ruptures, mass-wasting and landslides in the fields along the faults, the field investigations were limited to scattered sites and no information was obtained on the focal depth

Preprints (www.preprints.org) | NOT PEER-REVIEWED | Posted: 28 June 2018 doi:10.20944/preprints201806.0466.v1

distribution of the ruptured area. Geophysical studies were also inadequate for determining the spatial and temporal details of the aftershock clusters around the hypocenter of the mainshock (Utkucu et al. 2013; Bayrak et al. 2013; Fielding et al. 2013; Elliott et al. 2013; Moro et al. 2014). Furthermore, the land-based observations that were conducted were insufficient to describe the overall rupture geometry and the detailed hypocenter activity (Utkucu 2013; Kalafat et al. 2013; Altıner et al. 2013). Prior to the present study, little was known about the focal depth nature of aftershock seismicity at crustal depths.

Since the aftershocks following the Van and Edremit mainshocks occurred in larger numbers, they can assist in delineating the focal depth pattern of the rupture upon which the Van mainshock occurred and clarify the spatial and temporal distribution of the seismicity around the focal area. This paper explores the spatial and temporal distribution of the aftershock sequences in the Lake Van area to gain a better understanding of the hypocenter dynamics of aftershock sequence. Moreover, the current study analyzes the focal depth features of aftershocks beneath the surface based on aftershock observations and comments on rupture complexity of aftershock sequence, and contributes to the investigation of the distributional configurations of the hypocenters on the scale of a few tens of kilometers. This paper presents the results of the first detailed hypocentral observations and this is important data for future seismic hazard analyses in the area.

2. Data and Method

The earthquake catalogues published by AFAD (2011-2014) (Republic of Turkey Prime Ministry Disaster and Emergency Management Authority) ((http://www.afad.gov.tr/ and http://www.deprem.gov.tr/en/ddacatalogue) and by KOERI (2011-2014) (Boğaziçi University,

 doi:10.20944/preprints201806.0466.v1

Kandilli Observatory and Earthquake Research Institute) (http://www.koeri.boun.edu.tr/scripts/Sondepremler.asp) were used in the present study to plot the distribution of aftershocks and to propose a location uncertainty. This study used the routine procedure of the hypocenter location method given in the KOERI catalogue. The earthquake data set was manually analyzed using ZsacWin program of Yılmazer, (2003) developed at KOERI. The ZsacWin program is based on Hypo71 location software (Lee and Lahr 1972; Lee and Valdes, 1985) with 1-D crustal velocity models derived by Kalafat et al. (1987) for the hypocenter determination (further details are given in Appendix A).

AFAD operates 13 permanent broadband seismic stations equipped with high-gain seismometers around Lake Van and provides real-time data through on-line and dial-up stations. After the Van earthquake, 4 permanent broadband seismic stations were installed and operated by KOERI around Lake Van to record and locate the aftershock sequence (total 17 stations in Figure 1). It is possible to obtain reliable and acceptable focal depth solutions for any area of Turkey from earthquake data recorded at the digital broadband stations operated by the AFAD and KOERI using conventional and also inversion techniques.

The location uncertainty of routinely analyzed focal depths puts limits on the fine seismicity structure of the ruptured area. The use of a 1-D reference velocity models (Kalafat et al. 1987) to locate the focal depths limits the location accuracy due to systematic biases introduced by 3-D velocity variations. Several factors, such as the overall geometry of station network, arrival-times reading accuracy with available phases, and the crustal structure of the region, control the location accuracy of focal depths. However, relative focal depth location methods with 1-D velocity models can minimize the relative location uncertainties by controlling the accuracy of the relative arrival-time readings or selecting the high-quality events and the focal depths.

2.1 AFAD-KOERI joint catalogue

In this study, the catalogues from AFAD and KOERI networks (Fig. 1) have been merged in for quality check of the selected data. KOERI stations in the study area are not good enough to locate their own events. Hence, data (e.g., phase picks, phase readings and residuals) from nearby stations of KOERI network (see Appendix A) has been added to AFAD network to increase the resolution, to improve the location quality and also to compare the residuals. KOERI and AFAD networks have the schemes for automatically detecting events available for processing and working with the continuous data. These networks also provide arrival times and make corresponding hypocenter locations quite reliable for network well configured relative to the events (Fig. 1) (see Appendix B). The catalogues of AFAD and KOERI are well performed to improve the data quality and the depth resolution of the events given in the catalogues is refined. An important task here is to check phase picks and phase identifications to find possible large residuals from the different stations.

The hypocentral locations are the point with the best agreement between the observed and calculated times which means the root mean squared residual *RMS* given in location program and used as a guide to location accuracy and a criterion for “goodness of fit”. The *RMS* depending on the number of stations used in our study is reported by DDA catalogue of AFAD (http://www.deprem.gov.tr/en/ddacatalogue). DDA catalogue also has some scheme for weighting out large residuals. The point with the lowest *RMS* is assigned as the “solution” for well-behaved DDA catalogue. The residuals are of almost similar size in DDA catalogue, the

RMS gives the approximate average residual. We assume that the residuals caused by the crustal complexity are the same for all event-station pairs for various events. The residuals measured at relatively distant stations are almost similar for some events due to velocity variations outside the network that is suggested to cause individual station residuals.

In this study, the event locations and focal depths are well constrained due to both near and far stations (17 stations with location azimuthal gaps < 180º) (http://www.deprem.gov.tr/en/ddacatalogue/GetDDACatalogueSfile) (Fig. 1) using careful selections of only available P-phase reads at the nearest stations to get a reliable solution and to select high-quality events and the focal depths. The nearest stations influence very much on the accuracy of the data evaluation and provide the most accurate information due to the clarity of the phase reads. This gives a better fit and relatively correct location as an indication of the reliability of the inversion. However, the S-phase reads do not improve the solution and seem to have relatively large weights due to their lower velocities and possible local heterogeneities.

The AFAD-KOERI joint catalogue with selected events inside the network has P-residuals < 0.5 s. For distant stations, P-residuals from clear P-phases are less than 1 s while S-phases have relatively larger residuals due to structural complexities or their low velocities. These results show travel time residuals below AFAD-KOERI network and event-dependent values, depending on the network array, number of stations, event types and the number of secondary phases. In addition to residuals, epicenter locations, according to the faults observed from seismic reflection profiles (Toker and Şengör, 2011; Çukur et al., 2013; Çukur et al., 2016; Toker et al., 2017; Toker, 2017), are checked. Epicenters far outside the network and also S-phases are not used. The hypocenters are evaluated by low residuals and *RMS* that can ensure reasonable depths according to the appropriate action of the local operator. Thus, only the precisely located focal depths of aftershocks are used and relocated for analyses (see Appendix B). As a result, 1-2 km differences were obtained between the first solutions and horizontal and focal depth error.

In the present study, focal depth locations based on the AFAD-KOERI data set reveal a focused geometric picture of distributed aftershock seismicity (Toker, 2013; 2014; 2015) (Figs. B1 and B2). Most of the aftershocks align in upper crustal depths along curve-linear, linear, horizontal streaks. Most of the aftershock activity consists of clustered similar and/or same events, suggesting strong self-similarity of coupled events at depths with focal depth location errors typically about 1-2 km. Some selected events of the aftershock activity constrained by AFAD-KOERI joint catalog picks are also compared with the data set performed by previous studies (Gülen et al. 2002; Irmak et al., 2012; Kalafat et al., 2013; Fielding et al. 2013; Toker 2013; Bayrak et al. 2013; Toker 2014). The comparison indicates that overall geometric pattern of the individual events reveal the same relocated seismicity structure of Irmak et al., (2012) based on the same KOERI data set with focal depth uncertainties of 1-2 km (Irmak et al., 2012) and 2-3 km (Kalafat et al., 2013; Bayrak et al., 2013). This indicates reduced and desired location uncertainty in focal depths. Absolute uncertainties for aftershock locations are difficult to estimate because of the extreme structural complexity of the study area. However, considering that the structure is highly complex, and based on the hypocenter locations given in the AFAD-KOERI joint catalogue and also the data set performed by previous studies, this study proposes a focal depth location uncertainty of ~1-2 km.

2.2. Relocation results

The relocation results of the selected high-quality events based on the AFAD-KOERI joint catalog show that the seismicity has a maximum depth of ~30 km with peak activities at 8 and 10 km (Figs. B1 and B2). The relocated aftershocks more than about 65 % occur below ~10 km and indicate a focused view of the cluster seismicity at ~8-10 km, compared to the more scattered locations at AFAD network only (Fig. 1). Here, we conduct a spatial pattern analysis to address the distribution of the aftershock seismicity with respect to the basin-bounding faults (Fig. 2). The relocated aftershocks collapse into fault-bounding discrete zone within the Lake Van area (Fig. 2), and roughly follow the local zones of increased strains associated with the faults, while other located events became more spread out. Also, more aftershocks are densely positioned along the E-part of the lake, compared to the W-part. Seismic activity is increased to the E and S of the basin, while other areas remain seismically quite. When moving W in the basin along the boundary faults, the activity decreases and fades out, showing quite areas within the basin. However, the aftershock seismicity is densely distributed and clustered between the basin-bounding faults, when moving E in the basin. These observations indicate a clear “aftershock-clustered seismicity behavior” along the basin (Fig. 2). This is the basic pattern of our further analyses. These observations are also correlated with the multi-channel seismic reflection studies in Lake Van Basin (Çukur et al., 2013; Çukur et al., 2016; Toker et al., 2017; Toker, 2017) that indicate a tectonic mobility of cold, brittle and fragmentary crustal flake (tectonic model by Toker et al., 2017). This shows the clustered behavior of relocated aftershock seismic activity that almost reaches the upper elastic crust at about 10 km (Şengör et al., 1985; Dewey et al., 1986; Şengör et al., 2008; Toker et al., 2017; Toker, 2017) (Figs. A1 and A5) and the lower crust at about 30 km (Şengör et al., 2003; Şengör et al., 2008) (Figs. B1 and B2).

The earthquake catalog of the Lake Van study area, spanning the period November 2011–March 2014 and contains 10,000 events over three years. The depth and magnitude of the earthquakes ranged from 5 to 30 km and Mw 1.5–7.1, respectively. The relocated seismicity map of the Van mainshock-aftershock sequence for magnitudes (Mw ≥ 3.5) is well constrained by the previously mapped faults in Lake Van Basin (Çukur et al., 2013; Çukur et al., 2016; Toker et al., 2017; Toker, 2017), showing a sigmoidal pattern of aftershock distribution and the rupture zone parallel to the Lake Van tectonic trend and approximately 60-65 km in length (Figures 1 and 2). During the period 23 October, 2011 through November 2011 to December 2, 2011, the Van aftershock sequence consists of about 3100 events of (3.5 ≤ Mw ≤ 6.0) and the recorded events of magnitude Mw ≥ 4.0 were more than 100 occurred towards the north-east and south-west parts of the rupture area (Bayrak et al., 2013). These short-term records suggest that the seismic energy is mostly released in the form of moderate size aftershocks in the rupture area where large size asperities were found (Irmak et al. 2012; Bayrak et al. 2013).

The map view of the seismic density of the relocated aftershock hypocenters obtained from the AFAD-KOERI joint catalogue includes 5,088 events shown in Figure 2. In this study, ~150 days of aftershock data (from November 2011 to March 2012) were processed and projected from the catalogue. As a result, 4,853 aftershock hypocenters, of which 2,476 had a local magnitude greater than 3.5, were retrieved (Figures 3 and 4). In Figure 5, the cross-sections show the migrational patterns of the relocated hypocenter activity over the four periods including 4853 events of March 2012 as shown in Figure 3b. Then, to establish azimuth-dependent cross-sectional images of the aftershock distribution, the epicentral distribution of 10,000 events were selected for a time period from November 2011 to March 2014 (Figure 7). Finally, to plot the temporal distribution of the aftershocks and detect the temporal and spatial clustering of microseismicity, 6,135 events were selected from 282 days covering the period from October 23, 2011 to August 1, 2012 (Figures 8 and 9). Detailed images for depth-dependent P- and S-wave velocity anomalies and related cross-sections are given in Figs. A1-A5 and Figs. B1-B2, respectively.

2.3. Pattern recognition

The spatial and temporal patterns of the aftershock distribution associated with the observed clusters show no distinct difference between the periods of November 2011-March 2012 (Figures 3-6) and November 2011-March 2014 (Figure 7). The main difference is only related to the growing, tightening and deepening patterns of the observed clusters, showing a concentrated pattern of distribution and tightness of the relocated hypocenters. The hypocenter locations were compared to investigate the spatial and temporal variation of the seismicity in the clusters. The plotted hypocenter locations are closely and tightly spaced and clustered with the located clusters being densely concentrated. As a result, the pattern recognition of the clusters observed from aftershock relocation analyses is mainly based on the events concentration within highly distinct spatial activity (also see Figs. B1 and B2).

The closely located patterns of aftershocks recorded by a given station provide useful constraints in reducing the uncertainties involved in determining relative earthquake locations. The primary assumption that guarantees the usefulness of the clusters is that the hypocenters are closely spaced such that the observed waveforms of two close events are comparable due to the similarity in Green's functions, which characterize the source-receiver paths (An et al. 2010). This suggests that individual clusters show a high similarity of waveforms. However, there were thousands of aftershocks associated with many various and complex subpatterns of clusters in the current study, a waveform cross-correlation and/or a ST-clustering algorithm analysis were not carried out when locating the aftershocks. Detailed spatial pattern analyses of the observed clusters are not aimed in this study due to the presence of high quality, multi-channel seismic reflection and high-resolution Geo-chirp datasets collected from Lake Van Basin (Fig . 2) (Toker, 2011; Toker and Şengör, 2011; Çukur et al., 2013; Çukur et al., 2016; Toker et al., 2017; Toker, 2017) (see also Appendix A for Vp and Vs anomalies).

Overall pattern of larger main cluster was clearly observed from the 2011 Van event. This pattern was controlled by basin-bounding faults (Fig. 2) and caused by subsurface stress perturbations closely occurred at similar and smaller spatial scales (Toker 2014; 2015). Bayrak et al. (2013) reported that the irregular changes in b-value were extremely spatially localized. These results indicate that earthquakes occurring in very close vicinity to make a main cluster may represent the repeated slip of the same patch on a fault (Baisch et al. 2008; An et al. 2010). In the cross sections, the observed clusters are concentrated within highly distinct spatial activity and well constrained by the mapped basin-bounding faults (Fig. 2) (see Appendix B). The lower depth limit of seismicity in the main cluster was 8-10 km (Figures 4-6), but ~30 km (Figure 7), similar to the depths given in the previous studies. Thus, these observations indicate that the hypocentral accuracy and the location uncertainty of ~1-2 km in the focal depths are not considered to influence the discussion based on the main results presented in this study (see Appendix A and Appendix B).

3. Spatial and Temporal Character of the 23 October 2011 Aftershock Sequence

This section focuses on the spatial and temporal pattern of hypocenter distribution of the October 23, 2011 Van mainshock-aftershock events, being the largest shocks of that year in the region, and on the spatial and temporal characteristics of its aftershock sequence. This section aims to shed light on the focal depth nature of aftershock seismicity and the rupture complexity of the Van event.

3.1. Spatial and temporal distribution of aftershock hypocenters

The maps depicted in Figure 2 show the total distribution of 5088 aftershock events used in the first step of this study (AFAD-KOERI 2011-2014). Figure 2 is also the map view of seismic density of hypocenter distribution of the Van and Edremit aftershock sequences. That figure shows the sigmoid-like propagation of the rupture area corresponding to the aftershock sequences of the Van and Edremit mainshocks, with the boundary faults located around the epicenters of Van and Edremit events. The purpose of this section is simply to identify the cross-sections of the aftershock hypocenters associated with the map view given in Figure 2. To obtain a spatial and temporal overview of the seismicity pattern, the focal depth distribution of the aftershock hypocenters was examined month by month within the time period of November 2011 to March 2012. The results are presented in Figures 3a and 3b.

During the first month following the October 23 Van earthquake, different and various-sized clusters of local events occurred in the focal area (Figure 3). These aftershocks can be seen to have been gradually decaying over the subsequent months in the period up to March 2012 according to Omori's law (Omori 1884), and were dying out when the second Edremit event occurred (Figure 3a). In December 2011, the second month, the overall activity decreased continuing to decrease in the third and fourth months, and virtually ceased in the fifth month reaching 303 events (Figure 3a). In the same time period, November 2011 to March 2012, the total cumulative numbers of the aftershock activity increased (Figure 3b). Figure 3a shows that

 doi:10.20944/preprints201806.0466.v1

activity began to subside in March 2012, even though until the end of the July, 2012 there were several more events of $M \geq 4.0$ (Toker, 2014). The hypocentral superposition of aftershock events produced unusual seismic activity during the two last months of 2011 (Figure 3b). It appears that the Van earthquake repeatedly triggered one or more local faults in the area, and these in turn affected the seismicity.

In order to obtain more information from the distribution of hypocenters shown in Figure 3b to see and clarify the spatial patterns of the events distribution in detail different orientations of the focal area were tested, centering on the aftershock cloud, according to the focal mechanism given in Figure 2. The north-south trending zonal projections on the distribution of hypocenters associated with the Van event, starting with the west-east trending zonal distribution of the aftershocks for the four zones are shown in Figure 4. In this figure, the hypocenter distribution for each zone from narrow (zone 1) to wide (zone 4) indicates the first appearance of the small-sized linear clusters (zone 1) and uneven rapid concentration and densification of the event clusters (zone 2). Then, the hypocenter distribution defines a tightly consolidated and spherical (or semi-spherical) and/or parabolic pattern of the distribution (zones 3 and 4), which agrees with the distributional pattern given in Figure 3b.

3.2. The focal depth distribution of aftershock clusters

In Figure 4, the hypocenters of the aftershocks form a wide 'U' letter shaped cluster (hereafter referred to as the "main cluster"). This main cluster is a half cylinder-like channel-shaped cluster located at a broadly widening (about 60 km wide) area. The main cluster has a central (and/or core) cluster that is more tightly densified. The central cluster is narrow (about 25-30 km wide) bounded by faults f1 and f2 (Fig. 2) at south and north, respectively (Figure 4). The two arms of

Preprints (www.preprints.org) | NOT PEER-REVIEWED | Posted: 28 June 2018 doi:10.20944/preprints201806.0466.v1

the 'U' are symmetrically dip towards each other and are of almost the same length, about 20-30 km. The mainshock is included in the central part of the main and central cluster. The hypocenters belonging to the main cluster and its surrounding area have spans of about 25 and 30 km in the strike and dip direction, concentrated well into a depth of 8-10 km. Also, the hypocenters in the southern and northern part of the main cluster seem to be located along the extension of the plane of the central cluster aftershocks down to a depth of about 8-10 km.

The distributional pattern of hypocenters at the central cluster is fault-bounded (f1 and f2) (Fig. 2) and shows strong concentration in and around the focal area (Figure 4). However, the hypocenter activity outside the main cluster area deep down is more diffuse and few evident clusters can be seen. It is difficult to image the overall shape of the hypocenter distribution at a depth of more than 10 km due to the diffused and scattered focal depth distribution and do not seem to form a systematic pattern of the hypocenter geometry (Figure 4).

The overall distribution of hypocenters shown in Figures 3b and 4 is concentrated around the mainshock hypocenter and forms the central and main clusters. The most prominent aftershock cluster contains the mainshock hypocenter and has a U shape. The spatial extent of the plane of the concentrating aftershocks and their hypocenters indicate the location of the rupture area of the mainshock. The aftershocks on the periphery of the rupture area (zones 3 and 4 in Figure 4) show a more diffused distribution partly due to the off plane aftershock activity. The location of the plane of the aftershock distribution corresponds to the upper crustal seismicity. This location seems to be a good fit with the eastward and westward limit of the in-plane aftershock activity. The zonal correlation of the events distribution from narrow (zone 1) to wide (zone 4) given in

Figure 4 suggests that the shape of the upper crustal block controls the spatial extent of the asperity complex of the Van earthquake.

3.3. Migration of hypocenter activity

As shown in Figures 3 and 4, the spatial and temporal distribution of the aftershock seismicity can be explained through distinct cluster formations. The spatial and temporal variation of seismic activity is densely complex and highly clustered, comprising a repeated formation of small and large-sized clusters over brief time periods.

To further investigate the spatial and temporal variation of hypocenter activity in the main and central clusters shown in Figure 4 the hypocentral data was divided into four periods and different numbers of events for each period were used to reveal the migration and propagation of the hypocenter activity. Figure 5 displays the hypocenter activity of the March 2012 shown in Figure 3b and the distance versus depth plots for the four time periods are shown in each figure. The four periods shown in Figure 5 indicate the positions of the hypocenter activity for the cases of aftershock events of 662, 1,000, 2,000, 2,771, 3,000, 4,000, 4,402, and 4,853, respectively. Figure 5 reveals that the seismic activity began near the peripheral parts of the main cluster with small-sized linear clusters (a) and then migrated to the center and the north and formed the first traces of the central and main clusters (b) during the first period. The activity in the northern part started to accumulate in the center (c) and then, the activity jumped to the south during the second period. In the south, many aftershock events occurred, particularly larger events with magnitudes greater than 3.0-3.5 and the central and main clusters were apparently formed (d). During the third (f and e) and fourth periods (g and h), the hypocenters were distributed across entire clusters. Thus, the central and main clusters were tightly consolidated. In Figure 5, the

Preprints (www.preprints.org) | NOT PEER-REVIEWED | Posted: 28 June 2018 doi:10.20944/preprints201806.0466.v1

lower bound (seismicity front) of the main cluster increases over time, rapidly in the second period and this change in depth reaches 10-13 km. This parabolic-like envelope of the main cluster characterizes the diffusion-like front migration (g and h).

In the cross sections, the shallow and deep migration of hypocenter activity in the main and central clusters is shown in Figure 5. The hypocenters of more than 10 km seem to penetrate the deeper levels and those shallower than 10 km are located in the main and central clusters. The diffusivity is smaller inside the clusters and larger outside and towards the deeper levels. It can be inferred from the distance versus depth plots in Figure 5 that the migration and diffusivity of the hypocenter activity seems to increase over time from November 2011- March 2012, with the maximum diffusivity recorded in November 2011, when the seismic activity had increased drastically (2,828 events shown in Figure 3b). The general periodic trend of the migration of hypocenters and diffusivity implies that the aftershock activity accelerated during the second period of seismic activity for event numbers 2,000-2,771 (Figure 5). In Figure 5, the migrational pattern of hypocenter activity indicates spatially predominantly linear to planar hypocenter distributions in the first period, but quickly changes to parabolic to spherical (periods 2 and 3), and a more spherical spatial pattern in the last period. This suggests that the hypocentral variation of seismicity is not unidirectional but very complex.

To interpret the main and central clusters, the hypocenters of the 4,853 events are projected on the epicenters of the 5,088 events shown in Figure 6. The aftershock hypocenters are mainly distributed in the central section of the focal area. The main cluster is interpreted to be limited by the possible reverse faults f4 and f3 in south and north, respectively, while the central cluster is bounded by faults f1 and f2 (Fig. 2a). This suggests that the distributional pattern of the main and central clusters in the rupture area appears to be separated by fault-bounded crustal blocks (Fig. 2), which are initially proposed by Toker et al., (2017) and well constrained by Toker, (2017) based on the Gutenberg-Richter seismic b-values (see Figs. B1 and B2).

3.4. The Azimuth-dependent distribution of seismic activity

The spatial and temporal distributional patterns of the aftershock hypocenters were noted in the previous sections. To investigate their seismicity activity in greater detail, approximately 10,000 events were recorded in the time period from November 2011 to March 2014 (Figure 7). The epicenters and hypocenters were replotted using a rectangular-shaped analyse window (1.0º x 3.0º) to observe the azimuth-dependent changes of the aftershock seismicity projected on the distance versus depth plots. This is a very useful tool for investigating the hypocenters of events in the main and central clusters and their focal depth changes. Since the distribution of the seismic activity strongly depends on the azimuth and azimuthal rotation, the aftershock events located within the mainshock area are considered to be representative. For comparison, the aftershocks are shown using the azimuth-dependent projections.

Counterclockwise (-) and clockwise (+) rotational projections were applied to the events with rectangular-shaped analysis window of 1.0º x 3.0º. Hence, the azimuth-dependent rotation of the depth versus distance plots were used with varying rotation angles. The azimuth is 0º for the projections trending north-south, and ranges from -10° to -90°, for the counterclockwise rotation shown in Figure 7a and from +10° to +90° for the clockwise rotation given in Figure 7b, respectively. Then, the azimuth-dependent changes of the events are projected on the depth versus distance plots and shown along the lines of ten cross-sections (Figure 7).

The overall aftershock distribution on the cross-sections shown in Figure 7 roughly corresponds to the aftershock activity on those cross-sections (Figures 3-6). Along the azimuth-dependent projections, it can be seen that most of the hypocenter activity densely occurs just beneath the mainshock area and the central and main clusters are combined into the one unique and larger cluster at a depth of 30 km (Figs. B1 and B2). The cluster on the projections with an azimuth of 0º-40º and -50º-90º seems to have conical-shaped narrow and wide volumetric patterns, respectively (Figure 7a). These conical-shaped volumetric patterns of cluster seem to have the square-like widening patterns (Figure 7b). This suggests that the hypocenter activity migrates, extends down to ~25 km, with the maximum depth being 30 km and covers the whole crustal seismicity (Figs. A1-A4 and B1-B2). Given that the average cutoff depth of ~30 km represents the seismic base of the crust along the rupture fault system, the seismicity distribution indicates that the upper crust in the study area is brittle and seismogenic, and that the brittle–ductile transition may occur at the transition between the middle and upper crust. Since most of the aftershocks were found beneath the surface outcrops of the focal area and the basinal area of Lake Van with sparse aftershocks may represent the base of the thick sediment body.

The cross-section shown in Figure 6 is oriented south to north with 0º azimuth (see Figure 7). The hypocenters depicted on this cross-section show a possible convergence at depths of ~8-10 km (Figs. A1 and A5). The extrapolation of the central cluster from the surface is located around the mainshock surface rupture in the narrow area between Lake Van and Lake Erçek (faults f1 and f2 in Figure 6). Therefore, currently the central cluster is highly active and considered to represent the deep rupture associated with the mainshock and the main cluster appears to have been activated by the pre-existing low-angle reverse faults (f3 and f4). The cluster distribution suggests that the upper crust is so inhomogeneous and complex that an earthquake rupture would be an insufficient description based solely on the distributional pattern of the hypocenter. Basically, all the aftershocks are densely distributed around the main and central clusters, which confirm that the earthquake fault was ruptured during the Van earthquake.

3.5. Microseismicity clusters

This section further analyzes the spatial and temporal aftershock sequences occurring along secondary and/or splay faults at or along the fault-bounded (f1 and f2) central cluster shown in Figure 6. If the central cluster is currently highly active and considered to represent the deep rupture complexity, the close spatial and temporal proximity of microseismic events need to be used to improve the visual resolution of hypocenters in the central cluster. Hence, similar events were searched for using the temporal clustering procedure (Toker 2013; 2014) to locate the clustered microseismicity occurring within small volumes. Figure 8 shows the temporal distribution of aftershocks and temporal relation of the clustered events comparable to the magnitude and the focal depth versus time plots.

The temporal distribution of the aftershocks analyzed in this paper consists of a total of 6135 events over 282 days (October 23, 2011-August 1, 2012) in three different plots with Mw >1.5-2.0 earthquakes occurring sequentially one after another with the duration of each day being less than 24 hrs (Figure 8). In Figure 8, the prominent temporal activity sequence contains 60 events ($2.0 \leq Mw \leq 5.0$) occurring within the previous 16 days, with the strongest of the temporal activity clusters including 35 events ($2.0 \leq Mw \leq 4.0$) occurring within less than 12 hrs. The last individual temporal cluster was identified and analyzed, including the last 35 events. This cluster indicates that the temporal activity of the cluster is spatially concentrated within distinct activity events (Figure 8).

As shown in Figure 8, the most prominent sequence observed along the inferred fault consists of 60 located microearthquakes all occurring within 16 days preceding 31 July 2012 and within the ruptured area between Lake Van and Lake Erçek. This sequence indicates a west-east trending morphology of the inferred fault. The observed prominent temporal cluster consisted of 35 located microearthquakes that all occurred within a time period of less than 12 hrs on 1 August 2012 and within an area of about 2.5-3.0 km^2. The epicentral alignment of the events suggests an east-west striking orientation in the map view. The strike of the aligned events with the cluster and the local trend of the ruptured area suggest a junction between the main fault branch and a splay fault at the cluster (Figure 8). For a further analysis, the hypocenters of temporal cluster were plotted on a depth section trending north–south to observe the general trend of the events as identified in Figure 8. The 35 microearthquakes are observed that all occurred at the central cluster with varying depths (Figure 9). These events are linearly aligned in the section with the activity expanding to shallower depths, the hypocentral depths of the events range from 3.0 to 20 km, but remain limited to a depth of 20 km, and suggest a steep dip (≈ 90°) (Figure 9). The events were systematically spread along the plane of the section with a gradual increase of number of events during the most active part of the cluster. The largest event occurs with a magnitude of 4.0 and the centroid of the activity then migrates to the central cluster bounded by faults f1 and f2 (Figure 9). The hypocenters define the starting point of the cluster followed by a systematic migration throughout the central and main clusters shown in Figure 6.

The linear distributional pattern of the events cluster suggests vertical migration of the aftershock activity and most probably indicates the nucleation point of the failure between f1 and f2 and the progressive failure of adjacent patches of the possible fault (Figure 9). This was initiated on the central cluster and propagates vertically into the possible fault. The temporal distribution of the

 doi:10.20944/preprints201806.0466.v1

aftershock magnitudes, focal depths and the number of events observed within the cluster increased and then gradually decreased. The events cluster observed in Figure 9 represent the complex behavior of the rupture process within the central cluster.

4. Discussion

This paper reports on a study of the spatial and temporal character of the 2011 Van earthquake aftershock sequence with the following five aims. First, to identify the aftershock hypocenters and their spatial and temporal distributions linked to the mainshock and basin-bounding faults (f1 and f2) mapped from seismic reflection data in Lake Van Basin (Fig. 2a) (Toker, 2011; Toker and Şengör, 2011; Çukur et al., 2013; Çukur et al., 2016; Toker et al., 2017; Toker, 2017); second, to observe the aftershock clusters, their focal depth distributional patterns; third, to understand the migration of the hypocenter activity associated with each observed cluster; fourth, to determine the azimuth-dependent distribution of seismic activity; and fifth, to detect an individual temporal cluster of microseismicity along the ruptured area in the Lake Van area. Our analysis of the aftershock sequence leads to the result that the observed hypocentral activity, the main and central clusters and their surrounding events show distinct patterns of the distribution (Figs. A1-A5 and B1-B2). The spatial extent of the rupture area was fault-controlled extending from Lake Van Basin (Fig. 2) and found to be almost the same as the size of the aftershock distribution (Figures 3-6). These correspondences suggest that the aftershock distribution obtained by this study reflects an exact hypocentral picture of the crustal profile of the 2011 Van event (Figure 6).

4.1. Spatial and Temporal Character of the Aftershock Sequence

The overall pattern of the hypocenter distribution is seen to be terminated by the north- and south-trending arms of the U-shaped main cluster and the hypocenters north and south of the cluster show diffused focal depth distribution (Figures 4-6). This suggests that the north and south arms mark the up-dip limit of the rupture area of the mainshock. The aftershocks, at a depth of 8-10 km (Figures 5 and 6) and, up to 30 km (Figure 7) occur off the plane of the mainshock rupture. In Figure 7, the distributional pattern of the hypocenters extends more, to the deeper levels than the location of the main cluster as shown in Figures 5 and 6. This suggests that the coseismic slip distribution may be shifted compared to the previously determined hypocenter distribution. The aftershock activity may be inactive in the asperity region (e.g., the central cluster), where there is a large amount of coseismic slip (e.g., Scholz 2002, Hino et al. 2000). In the Van earthquake case, the aftershocks around the mainshock epicenter concentrated into large clusters and several areas of low seismicity may be the locations of the asperities ruptured by the mainshock (Yaginuma et al. 2005).

The northern and southern limits of the hypocenter distribution of the main cluster (Figures 4-6), which are interpreted as the northern and southern limits of the rupture area of the Van earthquake, correspond to the upper crustal-flake seismicity in eastern Anatolia (Dewey et al. 1986; Şengör et al. 1985; Şengör et al. 2008). The rupture propagation of the Van earthquake may be terminated by possible crustal fault planes (f3 and f4) located about 8-10 km up-dip of the hypocenter (Figure 6). This termination of the rupture propagation may have been caused by the reduction of the stress at the tips of growing faults by the seismic deformation spread over a broad zone, as shown in Figure 7 (King and Nablek 1985). It can be suggested that the intraplate

Preprints (www.preprints.org) | NOT PEER-REVIEWED | Posted: 28 June 2018 doi:10.20944/preprints201806.0466.v1

crustal seismicity (Toker, 2013) is activated along the west-east trending southern and northern arms of the main and central clusters (compare Figure 6 with Figure 7) as the result of the rupture termination process.

Toker (2015) reanalyzed seismic network data to compare the distributional pattern of the 4853 aftershocks (see Figures 3-6) with the 10,000 aftershocks (Figure 7) (Toker 2015) and the background seismicity pattern (Toker 2014). This comparison indicates that the positions of the active aftershock seismicity show spatial and temporal variations. That is, the positions of hypocenters and the overall geometric patterns of the clusters show the azimuth-dependent spatial variations along the distance versus depth plots (Figure 7). This may suggest seismic coupling and its spatial variations thus, implying that this seismic coupling is strongly controlled by the persistent temporal and spatial clusteral nature of the Van event (Toker 2014), such as structural heterogeneities, irregular strain accumulations, slip defects along or in the intraplate setting (Toker 2014; 2015). This reveals that the hypocenter distribution of the aftershock activity strongly reflects the spatial and temporal variation of the intraplate seismic coupling (Toker 2014).

The spatial and temporal clustering of microseismicity is also detected along the ruptured area in the Lake Van area (Figures 8 and 9). The hypocenter distribution of a single individual cluster represents an upward migration of microseismicity on an evolving subsidiary fault (Figure 9). The west-east trending fault morphology hosting cluster shown in Figure 8 forms part of the evolving fault network in the rupture area where the spatial and temporal distribution of the events are densely concentrated (Toker, 2017). The temporal clusters are associated with the earthquake sequences and frequently represent progressive failure of adjacent fault patches along

Preprints (www.preprints.org) | NOT PEER-REVIEWED | Posted: 28 June 2018 doi:10.20944/preprints201806.0466.v1

planes of activity (Toker 2013; 2014). These clusters are interpreted to represent repeated failure on the same source patch and considered to be hosted within the complex fault structures under non-uniform stress fields (Ben-Zion 2008; Toker 2013; 2014). This indicates that the spatial and temporal pattern of the events is associated with the currently active faults that display similar kinematics throughout the ruptured area (Çukur et al., 2016; Toker et al., 2017; Toker, 2017). This consists of a complex network of fault instabilities and/or patches connecting fluid-filled extensional cracks and/or fractures (Hill 1977). The central cluster shown in Figure 6 was correlated to the microseismicity cluster shown in Figure 9 finding that there was a spatial correlation between these clusters. The nature of seismic deformation energy released was assumed to be in a discrete form of spatial and temporal distribution of the aftershocks in and around the ruptured area (Toker 2014). This offers evidence of the temporal and spatial density of microseismicity clusters under the ruptured area, associated with discrete form of events due to the presence of disordered fault zones and high fracture density in the seismogenic crust (Bayrak et al., 2013; Toker 2013; 2015; 2017).

4.2. The rupture complexity of the Van earthquake

The analyses, in this paper, of the spatial and temporal character of the 2011 Van aftershock sequence are often associated with mapped faults in the Lake Van Basin (Fig. 2a) (Toker, 2011; Toker and Şengör, 2011; Çukur et al., 2013; Görür et al., 2015; Özalp et al., 2016; Çukur et al., 2016; Toker et al., 2017; Toker, 2017). The joint interpretation of aftershock sequence and seismic reflection profiles reveals the lateral and vertical heterogeneity of the fault-controlled aftershock distribution and along-strike seismic activity in crust within the rupture area. This suggests that the Van earthquake rupture process at crustal depths was not a simple frictional slip failure on the pre-existing, weak fault systems, but a more complex process that involved the fracturing of strong rock blocks (Bayrak et al., 2013; Toker, 2017). This means that the rupture area of the Van event is a fault-bounded fragmentation barrier (Toker, 2017). Such a local strong area (e.g., large asperity and/or barrier) is highly resistant to rupture growth on a fault and this area plays a more important role in determining the size of an earthquake than the remainder of the fault plane, which has little resistance to rupture growth (Ohnaka and Kato 2007; An et al. 2010). Moreover, hypocenters and their distributional patterns (e.g., the migration, diffusion, scattering and clusters) are also the consequence of stress redistribution related to the mainshock, occurring as failure along smaller fault asperities (Toker, 2017). Aftershocks involve lower stress values than the mainshock and thus, may occur at greater depths and over wider areas than the mainshock (Strehlau, 1986). In the present case, most of the aftershock hypocenters rapidly occurred and formed the clusters beneath the mainshock area, where the portion of the upper crust consists of the thrusted slices with volcanic materials (Şengör et al. 2003; 2008; Toker et al., 2017; Toker, 2017) and may contain asperities and barriers (Toker 2014). This may explain the spatial and temporal heterogeneity of the aftershock seismicity.

The anomalous distribution of larger aftershock activity in the Van mainshock also showed a triggered pattern of multi-clusteral events ($Mw \geq 4.0$) and extreme heterogeneity of the faulting in the rupture area (Toker 2013; 2014; 2015), supported by the large size asperities in the rupture zone of the mainshock (Irmak et al. 2012; Koçyiğit 2012). The short and long-term temporal activity of distinct clusters defined by Toker (2013; 2014) permits a better understanding of the rupture process in the local-scale seismicity along the ruptured area. Thus, the epicentral pattern of sequential events and hypocenters of microseismicity clusters supply important information by providing clues to the ruptured area (e.g., fracture, crack and permeability identification). The spatial and temporal distribution of microearthquakes and their systematic migration within individual clusters during the progressive failure of neighboring fault patches may define the simple picture of individual fault patches. Hence, the temporal pattern of seismic sequences observed in the ruptured area may suggest a progressive failure process on adjacent fault patches.

Considering the above results, the spatial and temporal character of the Van aftershock sequence is that the 2011 Van mainshock strongly triggered later events associated with a system of crustal faults along the accretionary wedge complex of Eastern Anatolia, and at the same time some crustal faults were activated reciprocally and new events were induced in the focal area. For example, the second destructive earthquake of Mw 5.6 (Edremit event) on November 9 was located on one of these faults, which probably had sufficient accumulated energy, and the stress storage derived from the adjustment of the tractions after October 23 acted as a trigger. The Van mainshock-aftershock sequence indicates the conditions under which aftershock events may interact with the other events (e.g., Edremit aftershock sequence) to repeat or renew the interactions of events (Toker 2013, 2014). The superposition of both the mainshocks within such a short interval of time with the respective aftershock sequences produced an intense spatial and temporal period of seismic activity that did not decay according to known simple laws.

4.3. Implications for the damaged area in and around Lake Van

The spatial and temporal character of the Van aftershock sequence associated with the mapped faults in Lake Van Basin reveals an increasing damage pattern with internal damage zones in the Lake Van area. The highly damaged rheology caused by the Van earthquake in multiple zones with a variable density of cracks/fractures/secondary smaller faults manifested as activated fields of intraplate stress heterogeneity (Toker 2013), reduced elastic moduli and increased dilatancy and anisotropy. These zones produced locally varying focal mechanisms and a high variance of the stress fields (Görgün 2013; Bayrak et al. 2013; Toker 2014).

The post-seismic hypocentral behavior of the Van aftershock sequence also exhibits distinct patterns of clusters and anisotropy in the distribution and redistribution of stresses over space and time (Toker 2013; Altiner et al. 2013). The damaged area from the Van event had a distinct asymmetric aftershock response to loading under heterogeneous stress conditions and clusters (also with decluster, quiescence and power-law truncation of events) during the loading-unloading intervals (Toker 2013). This was mainly due to a higher energy dissipation associated with the creation and activation of new small faults, microcracks and fractures (increasing damage) and the inelastic deformation of the internal damage zones (Ben-Zion 2008). These results imply that the asymmetry of the aftershock response to seismic deformation (damaged area) became extreme and strongly anisotropic across a wide range of size scales (wide ROSS) of the damage in the Lake Van area (Ben-Zion 2008; Toker 2013; 2014). This requires a view of the discrete framework commonly used in a statistical mechanics approach (Ben-Zion, 2008). The post-seismic hypocentral behavior of the Van aftershock sequence is, in fact, similar to the readjustment of crustal stresses (Khilyuk et al. 2000) in intraplate accretionary orogens (Şengör et al. 2003; 2008). This supports the argument that the real cause of the anomalous occurrence and distribution of aftershocks and their hypocenters may be anisotropic stress transfer and the rapid dynamic redistribution of stresses rather than the gradual static increase (Khilyuk et al. 2000; Ben-Zion 2008). This assumes a discrete structural model of the seismogenetic crust and suggests a dynamic origin of the 2011 Van mainshock-aftershock generation rather than the static concept of accumulated stresses (Toker 2014).

Preprints (www.preprints.org) | NOT PEER-REVIEWED | Posted: 28 June 2018 doi:10.20944/preprints201806.0466.v1

Previous studies of the 2011 Van event reported the heterogeneous stress and strain regimes in and around the focal area, however, they did not reveal how the seismic activity and related stress regime changed spatially and temporally. Several shallow faults observed in the field slipped for days and weeks after the mainshock. These shallower faults in the crust now have increased stress and were reported to have been triggered from the dynamic and static stress changes of the mainshock (Fielding et al. 2013). It can be postulated that spatial and temporal variations of the Van aftershock sequence, representing dynamical characteristics in the distribution of the spatial hypocenter locations of events, are related to changes in the high stress regimes. Our results show that the observed spatial and temporal variations in the seismicity are most likely due to significant changes in the local stress regime over an 2-year period (2011-2014), ranging from reverse-thrust faulting (fractures closing) via a strike-slip regime and finally to extensional faulting (fractures opening) (Irmak et al., 2012; Çukur et al., 2016; Toker et al., 2017; Toker, 2017). The detailed origins of these changes are not clear yet however, these results are critical for forthcoming large earthquakes. Despite the irresistant and warm crustal structure of the rupture area, the mid-crust behaved sufficiently strongly to rupture in the 2011 Van event and produce huge aftershock seismic activity. Thus, the Van earthquake and its long-period aftershock sequence are anomalously different from all the other earthquake types across Turkey.

5. Conclusions

This analysis of the spatial and temporal distribution of the 2011 Van earthquake aftershock sequence leads to the main conclusion that the observed hypocentral activity, the main and central clusters and their surrounding events show distinct distributional patterns of the rupture complexity of aftershock sequence. The aftershock distribution and its size reflect the spatial

Preprints (www.preprints.org) | NOT PEER-REVIEWED | Posted: 28 June 2018 doi:10.20944/preprints201806.0466.v1

extent of the rupture area and offer an exact hypocentral picture of the crustal profile of the 2011 Van event.

The overall distribution of hypocenters is concentrated around the mainshock hypocenter and forms two prominent clusters consisting of the central and main clusters. The main cluster bounded by possible reverse faults f4 and f3 seems to have been activated by the pre-existing low-angle reverse faults, while the central cluster bounded by faults f1 and f2 is currently highly active. The distributional pattern of both clusters in the rupture area appears to be separated by fault-bounded crustal blocks, representing the deep rupture. The migrational patterns of the hypocenter distribution indicate predominantly spatially linear to planar hypocenter distributions in the first period, but quickly changes to parabolic then to spherical, acquiring a more spherical spatial pattern in the last period. The location of the plane of aftershock distribution corresponds to the upper crustal seismicity and the zonal correlation of hypocenter distribution from narrow to wide suggests that the shape of the upper crustal block controls the spatial extent of the asperity complex of the Van earthquake. The spatial and temporal distribution of aftershock sequence with the observed clusters suggests that the hypocentral variation of seismic activity is not unidirectional but very complex and highly clustered, consisting of the repeated formation of small and large-sized clusters over brief time periods.

The most dense hypocenter activity occurs just beneath the mainshock area along the azimuth-dependent rotational projections. Only one, unique and larger cluster is observed in the projections at 30 km depth. Depending on the azimuthal rotations, the distributional pattern of this cluster ranges from the conical-shaped to the square-like narrow and widening volumetric patterns and covers the whole crustal seismicity. An individual temporal cluster of

Preprints (www.preprints.org) | NOT PEER-REVIEWED | Posted: 28 June 2018 doi:10.20944/preprints201806.0466.v1

microseismicity and its spatial distribution can be observed in the rupture area. The spatial and temporal distributional pattern of each microseismicity cluster represents the vertical migration of the aftershock activity on an evolving subsidiary fault and indicates the nucleation point of the failure between faults (f1 and f2) and the progressive failure of adjacent patches of the possible fault. The west-east trending fault morphology hosting cluster forms part of the evolving fault network in the rupture area. This cluster suggests the complex faulting behavior of the rupture process both within and through the central cluster.

The results from the current study show that the observed spatial and temporal variations of the Van aftershock sequence represent dynamic characteristics in the distribution of the spatial hypocenter locations of events and related to significant changes in the local stress regime over a three-year period. This indicates a rapid dynamic redistribution of stresses rather than their gradual static increase, suggesting the azimuth-dependent spatial variations of the intraplate seismic coupling along the distance versus the depth plots and anisotropic stress transfer through the occurring events. This study provides valuable insight into the spatial and temporal interaction of the Van aftershock events at various scales comparable to, or better than the earthquake source dimensions. Hence, this analysis of the spatial and temporal characteristics of the 2011 Van mainshock might a give a clue to understanding the seismogenesis in the area; however, this approach to the Van rupture complexity is still lacking in terms of various stress and strain sources. To improve our study, a promising approach is to undertake a high-resolution spatial analysis of a much larger number of events and clusters including volcano-magmatic and swarm activities.

Acknowledgments

The author thanks all the members of the Republic of Turkey Prime Ministry Disaster and Emergency Management Authority (AFAD, Turkey), the National Earthquake Monitoring Center (NEMC, Turkey) and the Kandilli Observatory and Earthquake Research Institute (KOERI, Turkey) for providing the continuous seismological data (DDA catalogue and Sfile documents) used in this study. The author is also grateful to; Prof. Dr. Ali Pınar (Boğaziçi University, KOERI, Turkey), Prof. Dr. Şakir Şahin (Suleyman Demirel University, Turkey), Prof. Dr. Esa Turunen, Prof. Dr. Elena Kozlovskaya (University of Oulu, Sodankylä Geophysical Observatory, Finland) for help in providing the opportunity to use the earthquake data and the seismological laboratory, Prof. Dr. G. Berkan Ecevitoğlu for providing the aftershock data monitoring FORTRAN code and commenting on concluding remarks of this study. The author offers sincere thanks to Prof. Dr. Sebastian Krastel (Kiel, Germany), the leader of the Lake Van Project seismic survey, for providing the multi-channel seismic reflection profiles (International Continental Drilling Program, ICDP-PaleoVan Project-2004 funded by Deutsche Forschungsgemeinschaft collected from Lake Van basin. Also, the author offers his greatest thanks to the editors and the two anonymous reviewers for their constructive comments and suggestions which helped improve the manuscript. Some of the figures were generated by the Generic Mapping Tools (GMT) code developed by Wessel and Smith (1998).

References

Altiner Y, Söhne W, Güney C, Perlt J, Wang R, Muzli M (2013) A geodetic study of the 23 October 2011 Van, Turkey earthquake. Tectonophysics 588:118-134. doi.org/10.1016/j.tecto.2012.12.005

Preprints (www.preprints.org) | NOT PEER-REVIEWED | Posted: 28 June 2018 doi:10.20944/preprints201806.0466.v1

An M, Feng M, Long C (2010) Deep ruptures around the hypocenter of the 12 May 2008 Wenchuan earthquake deduced from aftershock observations. Tectonophysics 491:96-104. doi:10.1016/j.tecto.2009.12.024

Baisch S, Ceranna L, Harjes H-P (2008) Earthquake cluster: what can we learn from waveform similarity? Bull. Seismol. Soc. Am. 98(6):2806–2814

Bayrak Y, Yadav RBS, Kalafat D, Tsapanos TM, Çınar H, Singh AP, Bayrak E, Yılmaz Ş, Öcal F, Koravos G (2013) Seismogenesis and earthquake triggering during the Van (Turkey) 2011 seismic sequence. Tectonophysics 601:163-176. doi:10.1016/j.tecto.2013.05.008

Benito B, Cepeda JM, Martinez Diaz JJ (2004) Analysis of the spatial and temporal distribution of the 2001 earthquakes in El Salvador. In: Rose WI, Bommer JJ, López DL, Carr MJ, Major JJ (eds) Natural hazards in El Salvador. The Geological Society of America Special Paper 375. Boulder, Colorado

Ben-Zion Y (2008) Collective behavior of earthquakes and faults: Continuum-discrete transitions, progressive evolutionary changes, and different dynamic regimes. Reviews of Geophysics. doi:10.1029/2008RG000260

Çukur D, Krastel S, Demirel-Schluter F, Demirbağ E, Imren C, Nissen F, Toker M, PaleoVan-Working Group (2013) Sedimentary evolution of Lake Van (Eastern Turkey) reconstructed from high-resolution seismic investigations. International Journal of Earth Sciences (Geol Rundsch) 102:571-585. doi:10.1007/s00531-012-0816-x

Çukur, D., Krastel, S., Tomonaga, Y., Schmincke, H.-U., Sumita, M., Meydan, A.F., Çağatay, M.N., Toker, M., Kim, S.-P., Kong, G.-S. & Horozal, S., (2016) Structural characteristics of the Lake Van Basin, Eastern Turkey, from high-resolution seismic reflection profiles and multibeam echosounder data: Geologic and tectonic implications, *Int. J. Earth Sci. (Geol Rundsch),* 106**,** 239-253.

Dewey JF, Hempton MR, Kidd WSF, Şaroğlu F, Şengör AMC (1986) Shortening of continental lithosphere: The neotectonics of Eastern Anatolia-a young collision. In: Coward MP, Ries AC (eds) Collision tectonics. Geological Society Special Publications, vol. 19. London, pp. 3-36

Doğan B, Karakaş A (2013), Geometry of co-seismic surface ruptures and tectonic meaning of the 23 October 2011 Mw 7.1 Van earthquake (East Anatolian Region, Turkey). J. Struct. Geol. 46:99-114

Doğan U, Demir DÖ, Çakir Z, Ergintav S. Ozener H, Akoğlu AM, Nalbant SS, Reilinger R (2014) Postseismic deformation following the Mw 7.2, 23 October 2011 Van earthquake (Turkey): Evidence for aseismic fault reactivation. Geophys. Res. Lett. 41:2334-2341. doi:10.1002/2014GL059291

Elliott JR, Copley AC, Holley R, Scharer K, Parsons B (2013) The 2011 Mw 7.1 Van (eastern Turkey) earthquake. J. Geophys. Res. Solid Earth 118:1-19. doi:10.1002/jgrb.50117

Emre O, Duman TY, Ozalp S, Elmacı H (2011) 23 Ekim 2011 Van depremi saha gozlemleri ve kaynak faya ilişkin on değerlendirmeler. MTA Jeoloji Etutler Dairesi. Ankara

Preprints (www.preprints.org) | NOT PEER-REVIEWED | Posted: 28 June 2018 doi:10.20944/preprints201806.0466.v1

Fielding EJ, Lundgren PR, Taymaz T, Yolsal-Çevikbilen S, Owen SE (2013) Fault-Slip source models for the 2011 M 7.1 Van Earthquake in Turkey from SAR Interferometry, Pixel Offset Tracking, GPS, and Seismic Waveform Analysis. Seismological Research Letters 84(4):579-593. doi: 10.1785/0220120164

Gorbatov A, Kennett BLN (2003) Joint bulk-sound and shear tomography for western Pacific subduction zones. Earth Planet Sci Lett 210:527–543

Görgün E (2013) The 2011 October 23 *M*w 7.2 Van-Erciş, Turkey, earthquake and its aftershocks. Geophysical Journal International 195(2):1052-1067. doi:10.1093/gji/ggt264

Görür N, Cağatay MN, Zabcı C, Sakınç M, Akkök R, Hande Ş, Örcen S (2015) The Late Quaternary Tectono-stratigraphic Evolution of the Lake Van, Turkey. Bull. Min. Res. Exp. 151:1-46

Gülen L, Pınar A, Kalafat D, Özel N, Horasan G, Yılmazer M, Işıkara AM (2002) Surface fault breaks, aftershocks distribution, and rupture process of the 17 August-1999 Izmit, Turkey, earthquake. Bulletin of the Seismological Society of America 92:230–244.

Harris RA, Simpson RW, Reasenberg PA (1995) Influence of static stress changes on earthquake locations in southern California. Nature 375:221-224

Hill DP (1977) A model for earthquake swarms. J. Geophys. Res. 82:347-352

Hino R, Ito S, Shiobara H, Shimamura H, Sato T, Kanazawa T, Kasahara J, Hasegawa A (2000) Aftershock distribution of the 1994 Sanriku-oki earthquake (Mw 7.7) revealed by ocean bottom seismographic observation. J. Geophys. Res. 105:21697-21710

Preprints (www.preprints.org) | NOT PEER-REVIEWED | Posted: 28 June 2018 doi:10.20944/preprints201806.0466.v1

Irmak TS, Doğan B, Karakaş A (2012) Source mechanism of the 23 October 603 2011 Van (Turkey) earthquake (Mw = 7.1) and aftershocks with its tectonic implications. Earth Planets Space doi:10.5047/eps.2012.05.002

Kalafat D, Kekovalı K, Akkoyunlu F, Ögütçü Z (2013) Source mechanism and stress analysis of 23 October 2011 Van Earthquake (Mw=7.1) and aftershocks. J Seismol. 18:371-384. doi:10.1007/s10950-013-9413-0

Kalafat D, Gürbüz C, Üçer SB (1987) Batı Türkiye'de Kabuk ve Üst Manto Yapısının Araştırılması. Deprem Araştırma Bülteni Sayı 59: 43–64 (in Turkish)

Karakaş A, Coruk Ö, Doğan B (2013) Engineering geologic assessment of the slope movements and liquefaction failures of the 23 October 2011 Van earthquake (Mw = 7.2). Nat. Hazards Earth Syst. Sci. 13:1113-1126. doi:10.5194/nhess-13-1113-2013

Ketin I (1977) A short explanation about the results of observations made in the region between Lake Van and Iranian border. Bulletin of Geological Society of Turkey 20:79-85

Khilyuk LF, Chilinger GV, Robertson JO, Endres B (2000) Gas migration: Events preceding earthquakes. Gulf Publishing Company Press, USA

King G, Nablek J (1985) Role of fault bends in the initiation and termination of earthquake rupture. Science 228:984-987

King GCP, Stein RS, Lin J (1994) Static stress changes and the triggering of earthquakes. Bulletin of the Seismological Society of America 84:935-953

Preprints (www.preprints.org) | NOT PEER-REVIEWED | Posted: 28 June 2018 doi:10.20944/preprints201806.0466.v1

Koçyiğit A (2012) New field and seismic data about the intraplate strike-slip deformation in Van region, East Anatolian plateau, E. Turkey. Journal of Asian Earth Sciences 62:586-605. doi:10.1016/j.jseaes.2012.11.008

KOERI (2011-2014) Boğaziçi University, Kandilli Observatory and Earthquake Research Institute. http://www.koeri.boun.edu.tr/

Kutoğlu HS, Toker M, Mekik C (2016) The 3-D Strain patterns in Turkey using Geodetic velocity fields from the RTK-CORS (TR) Network. Journal of African Earth Sciences 115:246-270. doi:10.1016/j.jafrearsci.2015.12.002

Lee WHK, Lahr JC (1972) HYPO71: a computer program for determining hypocenter, magnitude and first-motion pattern of local earthquakes, U.S. Geological survey open-file report, pp. 100

Lee WHK, Valdes CM (1985) HYPO71PC: A Personal Computer Version of the HYP071 Earthquake Location Program, USGS, Open File Report, pp. 1–28

Moro M, Cannelli V, Chini M, Bignami C, Melini D, Stramondo S, Saroli M, Picchiani M, Kyriakopoulos C, Brunori CA (2014) The October 23, 2011, Van (Turkey) earthquake and its relationship with neighbouring structures. Sci. Rep. doi:10.1038/srep03959

Ohnaka M, Kato A (2007) Depth dependence of constitutive law parameters for shear failure of rock at local strong areas on faults in the seismogenic crust. J. Geophys. Res. doi: 10.1029/2006JB004260

Preprints (www.preprints.org) | NOT PEER-REVIEWED | Posted: 28 June 2018 doi:10.20944/preprints201806.0466.v1

Omori F (1884) On the aftershocks of earthquakes. Journal College of Sciences, Imperial University 7:111-200

Özalp, S., Aydemir, B.S., Olgun, Ş., Şimşek, B., Elmacı, H., Evren, M., Emre, Ö., Aydın, M.B., Kurtuluş, O., Öcal, F., Can, A.Z., Yanmaz, M.N., Apa, R. & Duman, T.Y., (2016) Tectonic deformations in the quaternary deposits of the Lake Van (Edremit Bay), Eastern Anatolia, Turkey, *Bull. Min. Res. Exp.,* 153.

Paige CC, Saunders MA (1982) LSQR: sparse linear equations and least squares problems. ACM Trans Math Softw 8:43–71

Reasenberg P, Simpson R (1992) Response of regional seismicity to the static stress change produced by Loma Prieta Earthquake. Science 255:1687-1690

Salah, M.K., Şahin, Ş., Aydin, U., 2011. Seismic velocity and Poisson's ratio tomography of the crust beneath East Anatolia. Journal of Asian Earth Sciences 40 (2011) 746–761. doi:10.1016/j.jseaes.2010.10.021.

Salah, M.K., Şahin, Ş., Destici, C., 2007. Seismic velocity and Poisson's ratio tomography of the crust beneath southwest Anatolia: an insight into the occurrence of large earthquakes. Journal of Seismology 11, 415–432. doi:10.1007/s10950-007-9062-2.

Scholz CH (2002) The mechanics of earthquakes and faulting, 2nd edn. Cambridge University Press, Cambridge

Şengör AMC, Görür N, Şaroğlu F (1985) Strike-slip faulting and related basin formation in zones of tectonic escape. Turkey as a case study in Strike-slip faulting and basin formation. In: Biddle

KT, Christie-Blick N (eds) Strike-slip deformation, basin formation and sedimentation. Special Publication of Society of Economic Paleontologists and Mineralogists, vol. 37. Tulsa, Oklahoma, pp 227-264

Şengör AMC, Özeren MS, Genç C, Zor E (2003) East Anatolian high plateau as a mantle-supported, north-south shortened domal structure. Geophysical Research Letters 30(24):8045. doi:10.1029/2003GL017858

Şengör AMC, Özeren MS, Keskin M, Sakınç M, Özbakır AD, Kayan İ (2008) Eastern Turkish high plateau as a small Turkic-type orogen: Implications for post-collisional crust-forming processes in Turkic-type orogens. Earth-Science Reviews 90(1-2):1-48

Stein RS (1999) The role of stress transfer in earthquake recurrence. Nature 402:605-609

Stein RS, Lisowski M (1983) The Homestead Valley earthquake sequence, California: Control of aftershocks and postseismic deformations. Journal Geophysical Research 88: 6477-6490

Strehlau J (1986) A discussion of the depth extent of rupture in large continental earthquakes. In: Das S, Boatwright J, Scholz CH (eds) Earthquake source mechanics. American Geophysical Union. Washington, pp 131-145

Toker M (2013) Time-dependent analysis of aftershock events and structural impacts on intraplate crustal seismicity of the Van earthquake (Mw 7.1, 23 October 2011), E-Anatolia. Central European Journal of Geosciences. 5:423-434. doi: 10.2478/s13533-012-0141-8

Toker M (2014) Discrete characteristics of the aftershock sequence of the 2011 Van earthquake. Journal of Asian Earth Sciences 92:168-186. doi:10.1016/j.jseaes.2014.06.015.

Toker, M., Sengör, A.M.C., Demirel-Schluter, F., Demirbağ, E., Çukur, D., Imren, C., Niessen, F. & Group, P.-W., (2017) The structural elements and tectonics of the Lake Van basin (Eastern Anatolia) from multi-channel seismic reflection profiles, *J. Afr. Earth Sci.,* 129**,** 165-178.

Toker, M., (2017) The b-value analysis of aftershocks 170 days after the 23 October 2011 Van earthquake (Mw, 7.1) of the Lake Van basin, Eastern Anatolia: A new perspective on the seismic radiation and deformation characteristics. *in Earthquakes - Tectonics, Hazard and Risk Mitigation*, ed. Zouaghi, T.

Toker M, Ecevitoğlu GB (2012a) Van Gölü havzasının tektonik ve sismolojik özellikleri (6000 artçı deprem ve 180 günlük sismolojik ve sismotektonik modellenmesi), 1st edn. Anadolu University Publications, ISBN 978-975-06-1109-4, Eskişehir, Turkey (in Turkish)

Toker M, Ecevitoğlu GB (2012b) Shallow seismicity of the Van earthquake (M_L, 7.2, 23 October 2011, Eastern Anatolia): monitoring and analysis of the seismic data. In: Proceedings of the national conference with international participation "Geosciences 2012", Bulgarian Geological Society (BGS), Sofia, 13-14 December 2012

Toker M, Şengör AMC (2011) Van Gölü havzasının temel yapısal unsurları, tektonik ve sedimanter evrimi. Doğu Türkiye İTÜ Dergisi/D, Mühendislik 10(4):119-130

Toker M (2011) Tectonic and magmatic structure of Lake Van basin and its structural evolution, Eastern Anatolia Accretionary Complex (EAAC), E-Turkey. PhD thesis, Istanbul Technical University

Preprints (www.preprints.org) | NOT PEER-REVIEWED | Posted: 28 June 2018 doi:10.20944/preprints201806.0466.v1

Toker M (2015) Multi-clusteral nature of the 2011 Van earthquake aftershock sequence in the accretionary region of Eastern Anatolia. In: Efe R, Bizzarri C, Cürebal İ, Nyusupova GN (eds) Environment and ecology at the beginning of 21st century. St. Kliment Ohridski University Press, Sofia

Um J, Thurber C (1987) A fast algorithm for two-point seismic ray tracing. Bull Seismol Soc Am 77:972–986

Utkucu M (2006) Implications for the water-level-change triggered moderate (M≥4.0) earthquakes in Lake Van basin, Eastern Turkey. Journal of Seismology 10:105–117. doi: 10.1007/s10950-005-9002-y

Utkucu M (2013) 23 October 2011 Van, Eastern Anatolia, earthquake (Mw 7.1) and seismotectonics of Lake Van Area. Journal of Seismology 7(5):23-33

Utkucu M, Durmuş H, Yalçın H, Budakoğlu E, Işık E (2013) Coulomb static stress changes before and after the 23 October 2011 Van, eastern Turkey, earthquake (Mw = 7.1): Implications for the earthquake hazard mitigation. Natural Hazards and Earth System Science 13:1-14. doi: 10.5194/nhess-13-1-2013

Wessel P, Smith WHF (1998) New, improved version of the Generic Mapping Tools released. EOS 79:579

Yaginuma T, Okada T, Umino N, Hasegawa A (2005) Asperity of the 2005 off Miyagi earthquake (M7.2) estimated by waveform inversion [in Japanese]. Program Abstr. Seism. Soc. Japan, PM16

Yılmazer M (2003) Deprem kaynak parametrelerinin On-line Belirlenmesi. İstanbul Üniversitesi, Fen Bilimleri Enstitüsü, Yüksek Lisans Tezi, 47 s, İstanbul (Turkish)

Zhao D (2001) New advances of seismic tomography and its applications to subduction zones and earthquake fault zones: a review. Isl Arc 10:68–84

Zhao D, Kanamori H (1995) The 1994 Northridge earthquake: 3-D crustal structure in the rupture zone and its relation to the aftershock locations and mechanisms. Geophys Res Lett 22:763–766

Zhao D, Hasegawa A, Horiuchi S (1992) Tomographic imaging of P- and S-wave velocity structure beneath northeastern Japan. J Geophys Res 97:19909–19928

Zhao D, Hasegawa A, Kanamori H (1994) Deep structure of Japan subduction zone as derived from local, regional, and teleseismic events. J Geophys Res 99:22313–22329

Zhao D, Kanamori H, Humphreys E (1996) Simultaneous inversion of local and teleseismic data for the crust and mantle structure of southern California. Phys Earth Planet Inter 93:191–214

Zhao D, Xu Y, Wiens D, Dorman L, Hildebrand J, Webb S (1997) Depth extent of the Lau back-arc spreading center and its relation to subduction processes. Science 278:254–257

Zhao D, Wang K, Rogers G, Peacock S (2001) Tomographic image of low P velocity anomalies above slab in northern Cascadia subduction zone. Earth Planets Space 53:285–293

Preprints (www.preprints.org) | NOT PEER-REVIEWED | Posted: 28 June 2018 doi:10.20944/preprints201806.0466.v1

APPENDIX A.

A close spatial inspection of the clusteral pattern of aftershock distribution at depths of 10 km up to 30 km implies a possible relation between the fault-controlled nucleation zone of 2011 Van earthquake aftershock sequence and P- and S-wave velocity anomalies. This relation seems to be due to crustal faulting movements along the Lake Van area, as was explained in the tectonic model study of Toker et al., (2017) and also Toker, (2017).

The diffuse and asymmetric distributional pattern of aftershock events associated with the low number of stations may impose a few limitations on the resolution of the observed velocity amplitudes; the numbers of aftershock events are very sparse and the seismicity level is low in the S-, W- and central parts of the lake. However, aftershocks are densely clustered in the E- and NE-parts of the lake. The large number of data and the good ray crisscrossing in clustered area (main/central cluster) of the lake can provide the reliability of the obtained velocity anomalies (Gorbatov and Kennett 2003) and their possible relation to the main/central cluster. Therefore, in this section, the main results of our study are qualified by applying a different approach. The selected aftershock events and their focal depths are re-examined and data interpretation is revised and integrated with seismic velocity anomalies to reveal the velocity structure of the main/central cluster and improve the main results of this study.

A number of 15,760 events selected between 2007 and 2016 (37 – 40°N and 41 – 45°E) generated 76,160 P- and 31,641 S-arrivals recorded by 22 seismic stations (from the Seismic Network of Regional Earthquake-Tsunami Monitoring Center operated by KOERI), implying the similar ray coverage patterns of both P- and S-wave data sets. The network has 21 broadband and 1 short-period seismic stations with a sampling frequency of 50 Hz. The dynamic range is 140 and 164–184 dB for the broadband and short-period seismic stations, respectively. The Hypo71 source code and the velocity model of Kalafat (1987) are used for the determination of the hypocentral parameters (Lee and Lahr 1972). The errors in the hypocentral locations are ≈ 2 km. The accuracy of arrival times of P waves is estimated to be less than 0.15 s. Based on the initial velocity model, all residuals are stepwise examined. Residuals more than the limit ±1 s are excluded from the inversion.

The tomography technique of Zhao et al. (1992) is applied to the study area and is used to analyze the arrival times of P- and S-waves. This technique is easily applicable to 3-D complex velocity variations (e.g., clusters) in the model (Zhao and Kanamori 1995; Zhao et al. 1996, 1997, 2001; Salah et al., 2007, 2011). Velocity perturbations at the nodes of 3-D grid net are assumed as unknown parameters. The velocity perturbation at any point can be calculated by linear interpolation of the velocity perturbations at the eight grid nodes surrounding that point. The 3-D ray-tracing technique by Zhao et al. (1992) is employed to calculate travel times and ray paths accurately. The ray-tracing iteratively uses the pseudobending technique (Um and Thurber 1987) and Snell's law. The observation equations are solved by using the least squares regression algorithm given by Paige and Saunders, (1982) with a damping regularization. Conducting linear inversions iteratively solve the nonlinear tomographic problem (see Zhao et al., 1992; 1994 and Zhao, 2001 for a detailed description of the technique).

A grid spacing of 0.5° x 0.5° in the horizontal scale and that of 0–5 km in the vertical scale is adopted. Four layers of grid nodes are set up at 4-, 7-, 14-, and 23-km depths due to enough ray coverage pattern at these four depth layers in which the number of P- and S-wave ray hit counts at each grid node is assumed to be adequate to retrieve the velocity anomalies (grid nodes at depths of < 4 km are ignored). Grid nodes with hit counts of less than 10 are not included in the inversion. The E- and NE-parts of the study area have large hit counts and many nodes are hit by more than 5000 rays at the first two crustal layers. An initial S-wave velocity model was calculated by assuming a constant Vp/Vs value of 1.73 (Vp/Vs value from KOERI). The obtained value of Vp/Vs ratio indicates almost constant velocity model structure, but with a few slight changes in the edges, suggesting the reliability of the Vp/Vs ratio in most cases (≈ 1.73). The velocity anomalies of 4% are alternatively assigned to the 3-D grid nodes to create a checkerboard pattern; the image of which is straightforward and easy to remember. Random errors of 0.1–0.15 s, similar in magnitude to those of the real data, are added to the synthetic arrival times and are then inverted with the same algorithm used for the real data inversion. The checkerboard resolution test indicates a good and uniform resolution of about 30 km horizontally for the two data sets in the Lake Van and its vicinity, especially at 4- and 23-km depths. Applying the tomographic technique to the data set, the sum of squared travel-time residuals is reduced by more than 30% of its initial value after the inversion process. The final RMS travel time residuals are 0.49 s and 0.52 s for the P-wave, and S-wave data sets, respectively.

Tomographic imaging of P-wave velocity structure beneath main/central cluster at depths of 10, 14, 18, 23 km (Figs. A1-A4) and S-wave velocity structure at a depth of 10 km (Fig. A5) is performed to indicate velocity-dependent structural pattern of main/central cluster. The distributions of Vp and Vs are well recovered down to crustal depths at which the cluster is observed. This indicates that the velocity anomalies from the inverted P- and S-waves are considered to be reliable within and nearby the central/main cluster at depths of 10 km up to 30 km. The velocity perturbations in percentage from the initial velocity model at each depth are also deduced from the inverted 3-D model.

Preprints (www.preprints.org) | NOT PEER-REVIEWED | Posted: 28 June 2018 doi:10.20944/preprints201806.0466.v1

P- and S-wave velocity anomalies and their relation to structural pattern of main/central cluster are revealed by the following images (Figs. A1-A5). Generally, low Vp and Vs anomalies slightly change to high Vp and Vs at cluster depths and are densely concentrated within the main/central cluster at which the seismic activity is very intense with low-V, low- to high-V.

APPENDIX B.

S-N cross-sectional depth profiles of Vp-%Vp and Vs-%Vs distributions are projected on the main/central cluster (events with Mw ≥ 4.0 are selected only and shown in Figs. B1 and B2). The cross-sections show very distinct clusteral pattern of relocated events and velocity-dependent structure of the main/central cluster at depths smaller than 30 km.

In our study, the seismic velocity structure of the main/central cluster as a function of depth is imaged by tomographic inversion of P and S waves (Figs. A1-A5 and B1-B2). Distributional pattern of velocity anomalies are well consistent with clusteral pattern of relocated aftershock events (Mw ≥ 4.0). Velocity patterns for each depth interval are typically characteristics to overall structure of the main/central cluster. The cluster activity is very intense along highly heterogeneous focal zone characterized by low to high P- and low S-wave velocity anomalies, suggesting that the 2011 Van event and its aftershock sequences are well concentrated and densely consolidated within a zone bounded by low, and low to high velocities. These results indicate that the observed velocity anomalies and their relations to structural pattern of main/central cluster are reliable features down to depths of, at least, 10 km and 30 km, at which the main/central cluster is prominently seismically active.

Preprints (www.preprints.org) | NOT PEER-REVIEWED | Posted: 28 June 2018 doi:10.20944/preprints201806.0466.v1

Figure Legends

Figure 1 Seismicity of the Lake Van area and all 5,088 aftershock distributions of the 23 October 2011 Van (*Mw 7.1*) and 9 November 2011 Edremit (*Mw 5.6*) earthquakes. The epicenters of the aftershock occurred until April 2012 are plotted. The colored dots denote the aftershock magnitudes determined by the AFAD-KOERI seismic network (the inset map). The station locations of AFAD (13 stations shown by yellow color) and KOERI (4 stations shown by red color) networks are used for the distributional analyses of the aftershocks relocated in this study. The relocated epicenters show a compact and sigmoidal distributional pattern.

Figure 2 Shaded relief maps of the focal depth distribution of the relocated aftershock hypocenters (5088 events) shown in Figure1 in the ruptured area. The Lake Van boundary faults used to constrain the focal depth data are also shown (data compiled from Toker 2011; Toker and Şengör 2011; Çukur et al. 2013; Çukur et al. 2016; Toker et al., 2017; Toker, 2017). The map in **a** shows aftershock distribution, the fault plane solutions of the Van and Edremit mainshocks (numbers 1 and 3) and 20 aftershocks of the Van earthquake with the hypocenter depths occurring during the earthquake (fault focal mechanism solutions compiled from Irmak et al. 2012 and various institutions) (Görgün 2013; Toker 2013; Bayrak et al. 2013; Toker 2014). The numbers on the map and the focal mechanisms indicate these aftershocks. Local faults (f1, f2) are the landward continuations of basin-bounding faults in Lake Van (see tectonic and seismic b-value models by Toker et al., 2017 and Toker, 2017, respectively). The map in **b** indicates the relation of the faulting styles of the lake to the distributional density of the hypocenters. Contours are depths in km. The dots denote the aftershock epicenters. Dashed black line is common cluster axis. The maps indicate that seismic density of the located hypocenters is concentrated along a

Preprints (www.preprints.org) | NOT PEER-REVIEWED | Posted: 28 June 2018 doi:10.20944/preprints201806.0466.v1

landward extending sigmoidal pattern corresponding to the ruptured area and the faulting style in the lake. The normal and thrust focal solutions seen in **a** are related to the rupturing of the secondary faults as a result of the rupturing of a main thrust fault plane in the NE direction and with a 58◦NW dip (Irmak et al. 2012). The rupturing caused secondary intra-plate deformations obtained from the fault plane solutions of the aftershocks numbered 22 on map and fits with the direction of the aftershock pattern (focal data compiled from Irmak et al. 2012).

Figure 3 Distance versus depth plots of distribution of all 4,853 aftershocks of the Van mainshock, for one month intervals from November 2011 to March 2012. The solid line labeled N–S in the map indicates the central line of the given cross-sections, and the solid square marks the 70-km-wide zone projected onto the cross-sections. Aftershocks within the squared area from the central line of the cross-section are projected onto the plane of the cross-section with the projected distance of 180 km. **a** Omori's law of decay of aftershocks identified as changing the aftershock events for each month over a five-month period are represented in their corresponding time windows. **b** Distance versus depth plots of distribution of the aftershocks within the time period from November 2011 to March 2012, with the cumulative numbers of the events for each month and the same representation criteria as in Figure 3a. F: the major regional thrust fault, f1: local thrust fault (Emre et al. 2011), f2: inferred local fault, local faults (f1, f2) are the landward continuations of basin-bounding faults in Lake Van (see tectonic model by Toker et al., 2017).

Figure 4 Distribution of all the 4,853 aftershocks along four vertical cross-sections, with a projected distance of 180 km. The aftershocks are presented as the areal distributions from narrow to wide zones as shown in the map. The solid rectangles labeled 1, 2, 3, and 4 indicate the W-E extending zones from the central line of the cross-sections, and the solid square marks the

Preprints (www.preprints.org) | NOT PEER-REVIEWED | Posted: 28 June 2018 doi:10.20944/preprints201806.0466.v1

70-km-wide zone projected onto the cross-sections. Aftershocks within the different zones from the central line of the cross-section are projected onto the plane of the cross-section. The locations of the cross-sections and the areas within the projected distances are also shown. Zones 1, 2, 3, and 4 contain 660 events, 2,762, 4,383, and 4,853, respectively. The distributional pattern of aftershocks in zone 4 is the same as for March 2012 in Figure 3b. F: the major regional thrust fault, f1: local thrust fault (Emre et al. 2011), f2: inferred local fault, local faults (f1, f2) are the landward continuations of basin-bounding faults in Lake Van (see tectonic model by Toker et al., 2017).

Figure 5 Distribution of all the 4,853 aftershocks along eight vertical cross-sections, with a projected distance of 180 km. The hypocenter distribution of the aftershocks is subdivided into the four periods. Aftershocks within the area from the central line of the cross-section shown in Figure 3b are projected onto the plane of the cross-section, for each of the four periodic distributions. Each period shows the evolutionary distribution of the central and main clusters from periods 1 to 4. The distributional pattern of aftershocks in the fourth period is the same as in March 2012 in Figure 3b and zone 4 in Figure 4. F: the major regional thrust fault, f1: local thrust fault (Emre et al. 2011), f2: inferred local fault, local faults (f1, f2) are the landward continuations of basin-bounding faults in Lake Van (see tectonic model by Toker et al., 2017).

Figure 6 Distribution of 4,853 events from all 5,088 epicenters in the shaded relief map along the vertical cross-section, with projected distance of 180 km. Aftershocks within the area from the central line of the cross-section are projected onto the plane of the cross-section. The distributional patterns of aftershocks and the clusters are the same as in the fourth period in Figure 5. F: the major regional thrust fault, f1: local thrust fault (Emre et al. 2011), f2: inferred

Preprints (www.preprints.org) | NOT PEER-REVIEWED | Posted: 28 June 2018 doi:10.20944/preprints201806.0466.v1

local fault, f3 and f4: inferred local thrust faults, local faults (f1, f2) are the landward continuations of basin-bounding faults in Lake Van (see tectonic model by Toker et al., 2017).

Figure 7 a Azimuth-dependent, counterclockwise (-0º to -90º), and **b** clockwise (+0º to +90º) distribution of all 10,000 aftershocks (November 2011-March 2014) along ten vertical cross-sections, with projected distances of 300 km. Aftershocks within the rectangle analysis window (1.0º x 3.0º-wide zone) from the central line of the cross-section are projected onto the plane of the cross-section and presented as a function of azimuths for each cross-sectional profile. The locations of the cross-sections and the area within the projected distance of 70 km are also shown.

Figure 8 Temporal distributional pattern of 6,135 aftershocks from 23 October 2011 to 1 August 2012 over 282 days with the daily seismicity rate, focal depths and magnitudes along the rupture area. A high number of events compared to the background seismicity can be seen for particular time periods indicating the temporal clustering of earthquakes along the rupture area (see Toker 2013; 2014; 2015 for temporal clusters over the whole data). Cumulative magnitudes of aftershock distribution do not exceed the commonly observed maximum magnitudes despite the very high number of events for 282 days. The last 60 events ($2 \leq Mw \leq 5$) during the last 16 days mark the most prominent sequence detected, while this sequence indicates a west-east trending inferred fault morphology along the rupture area (dashed red line). On the map, these 60 events are shown in numerical order according to the time of occurrence. The second prominent sequence marks the microseismicity cluster (C) also detected, containing the largest number (35 events) of the last events ($2 \leq Mw \leq 4$) indicating the spatial pattern of events cluster in the map. On the map, these 35 events are shown in numerical order according to the time of occurrence.

Preprints (www.preprints.org) | NOT PEER-REVIEWED | Posted: 28 June 2018 doi:10.20944/preprints201806.0466.v1

The map confirms the close spatial proximity of the microseismic events within the temporal cluster. LE: Lake Erçek.

Figure 9 Depth cross-section of the microseismicity cluster (C) shown in Figure 8 indicates the vertical hypocentral distribution with a dip angle of ~90°. The map shows the spatial distribution of C consisting of 35 located events (also see Figure 8, C for location). In the map, these 35 events are shown in numerical order according to the time of occurrence. Most events of the cluster occurred on a possible secondary fault (splay fault) close to the inferred fault (dashed red line) between f1 and f2 (central cluster). F: the major regional thrust fault, f1: local thrust fault (Emre et al., 2011), f2: inferred local fault, local faults (f1, f2) are the landward continuations of basin-bounding faults in Lake Van (see tectonic model by Toker et al., 2017), LE: Lake Erçek.

Figure A1. The distribution of Vp and %Vp (recovered down to 10 km depth) within and nearby the central/main cluster at depth of 10 km ranges between 7.05-7.25 km/s and -2 and -5, respectively.

Figure A2. The distribution of Vp and %Vp (recovered down to 14-km depth) within and nearby the central/main cluster at a depth of 14 km ranges between 7.05-7.3 km/s and between -3 and -5, respectively.

Figure A3. The distribution of Vp and %Vp (recovered down to 18-km depth) within and nearby the central/main cluster at a depth of 18 km ranges between 7.05-7.3 km/s and between -3 and -5, respectively.

Preprints (www.preprints.org) | NOT PEER-REVIEWED | Posted: 28 June 2018 doi:10.20944/preprints201806.0466.v1

Figure A4. The distribution of Vp and %Vp (recovered down to 23-km depth) within and nearby the central/main cluster at a depth of 23 km ranges between 7.28-7.46 km/s and between -1 and -4, respectively.

Figure A5. The distribution of Vs and %Vs (recovered down to 10-km depth) within and nearby the central/main cluster at a depth of 10 km ranges between 3.96-4.06 km/s and between -1 and -4, respectively.

Figure B1. Distance versus depth plots of distribution of Vp (left) and Vs (right) within and nearby the main/central cluster range between 6.8-7.6 km/s and 3.7-4.3 km/s, respectively.

Figure B2. Distance versus depth plots of distribution of %Vp (left) and %Vs (right) within and nearby the main/central cluster range between -1 and -6.

Preprints (www.preprints.org) | NOT PEER-REVIEWED | Posted: 28 June 2018 doi:10.20944/preprints201806.0466.v1

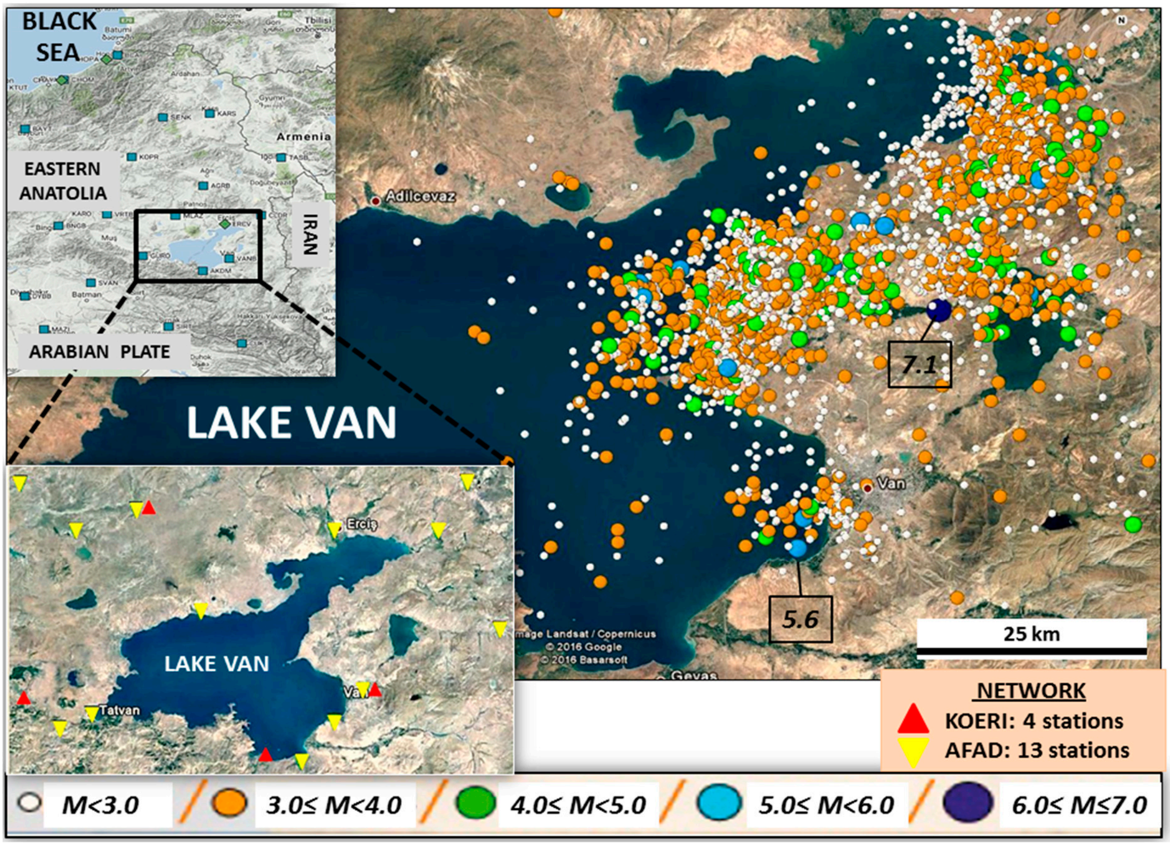

Fig. 1

Preprints (www.preprints.org) | NOT PEER-REVIEWED | Posted: 28 June 2018 doi:10.20944/preprints201806.0466.v1

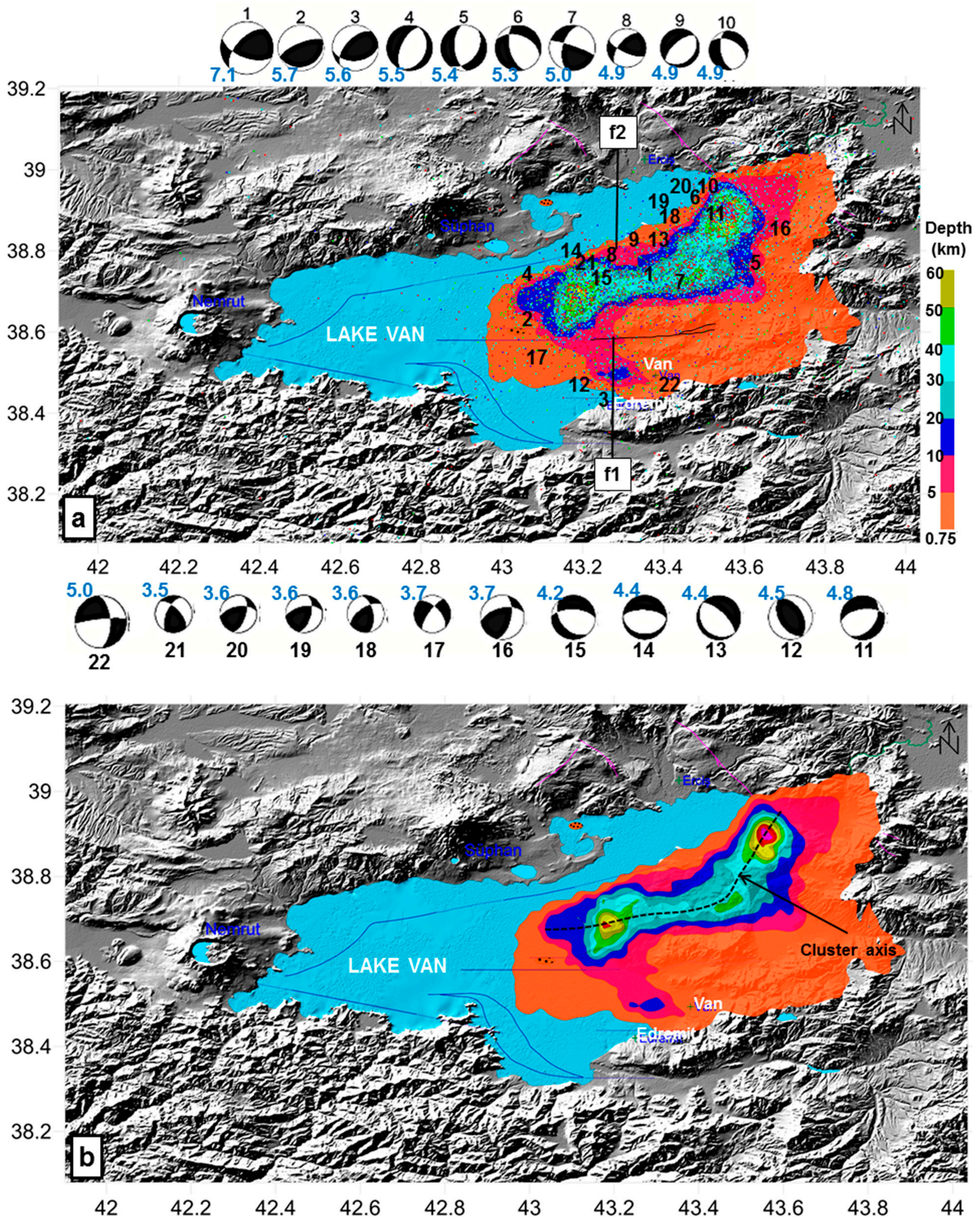

Fig. 2

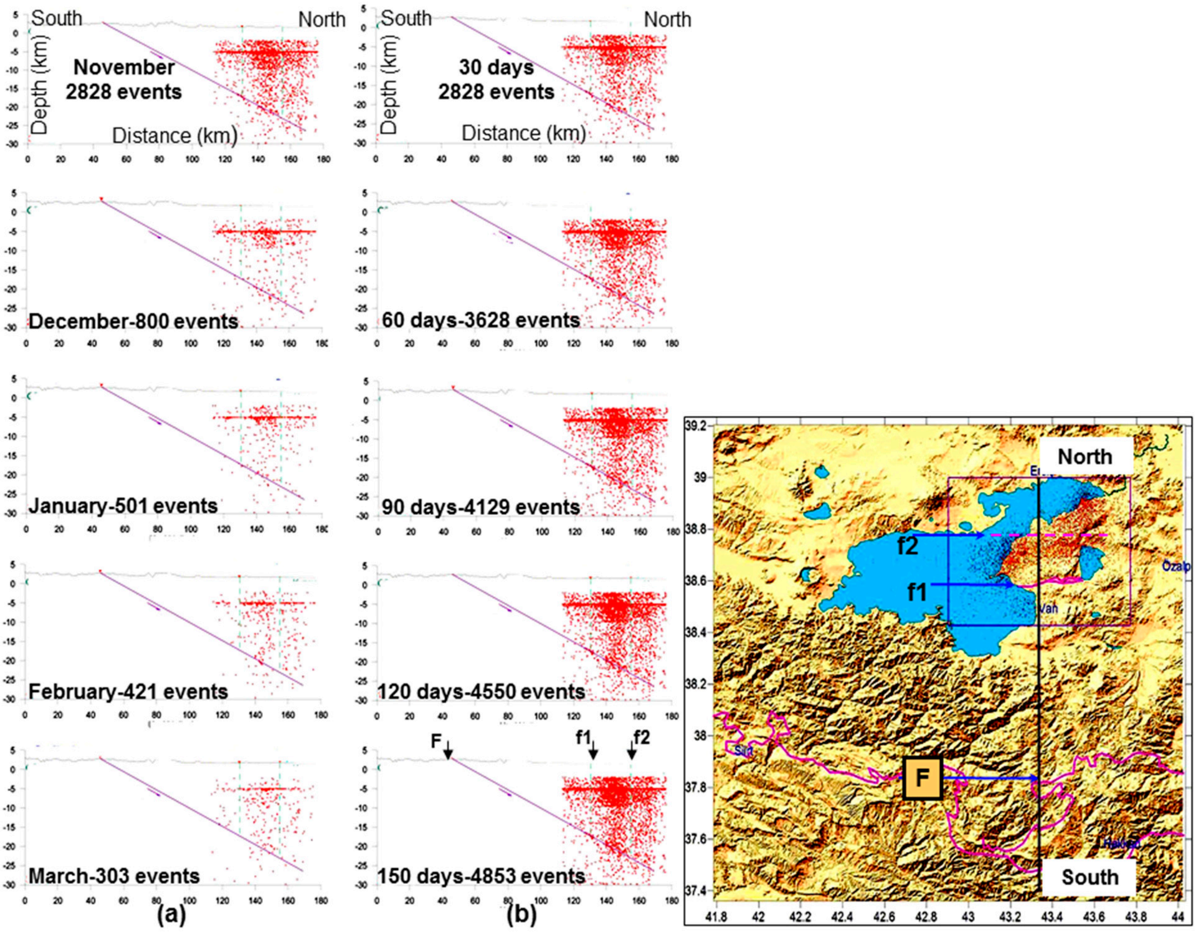
South
North
Depth (km)
November
2828 events
Distance (km)
30 days
2828 events
December-800 events
60 days-3628 events
January-501 events
90 days-4129 events
February-421 events
120 days-4550 events
March-303 events
150 days-4853 events
F
f1
f2
(a)
(b)
North
South
F
f1
f2

Fig. 3

Preprints (www.preprints.org) | NOT PEER-REVIEWED | Posted: 28 June 2018 doi:10.20944/preprints201806.0466.v1

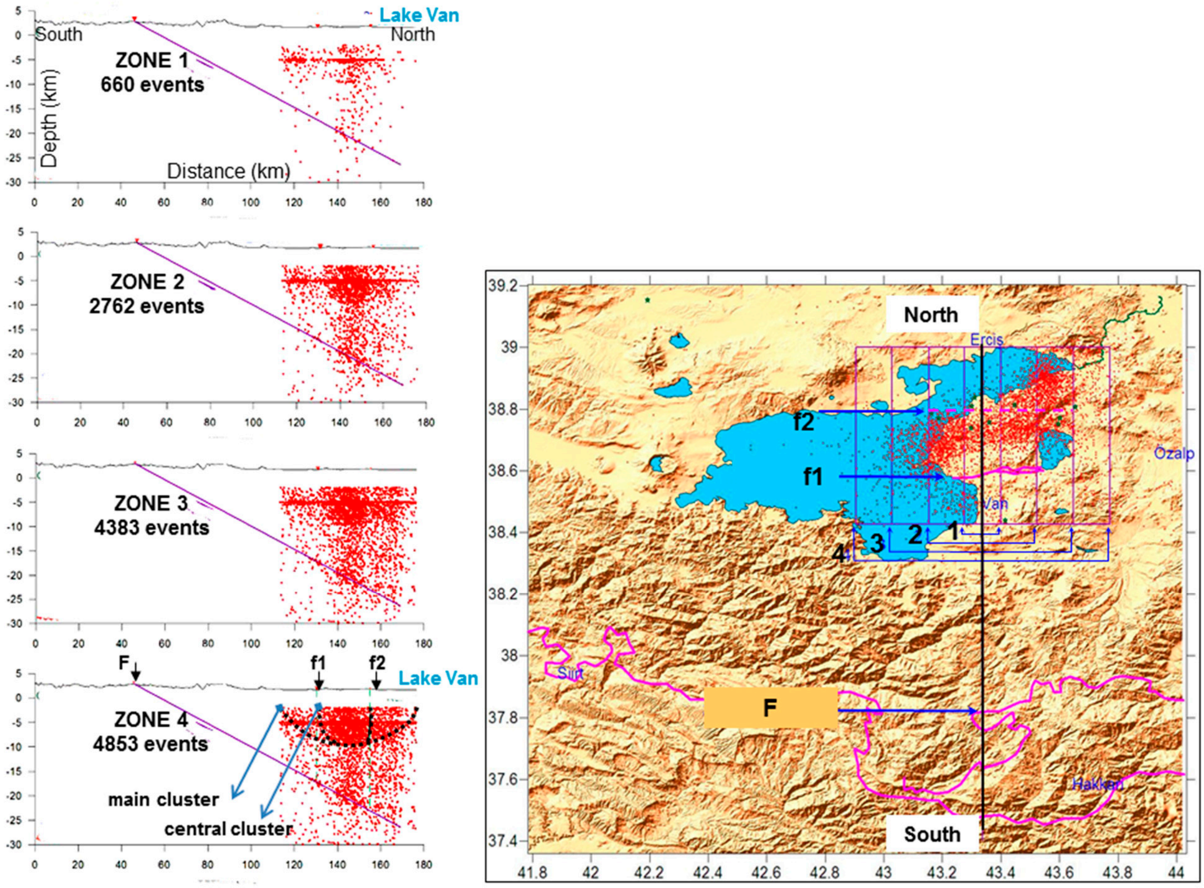

Fig. 4

doi:10.20944/preprints201806.0466.v1

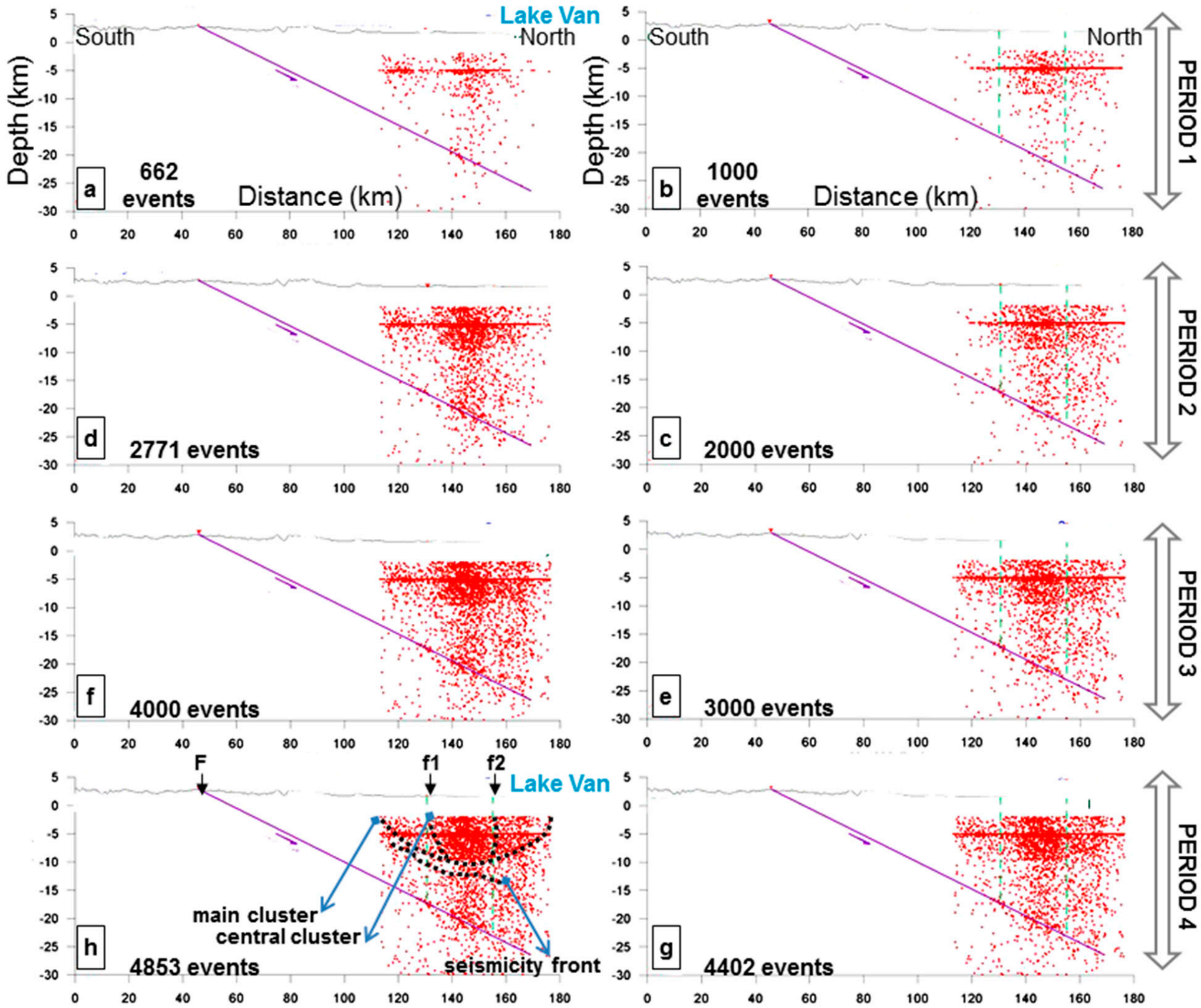

Fig. 5

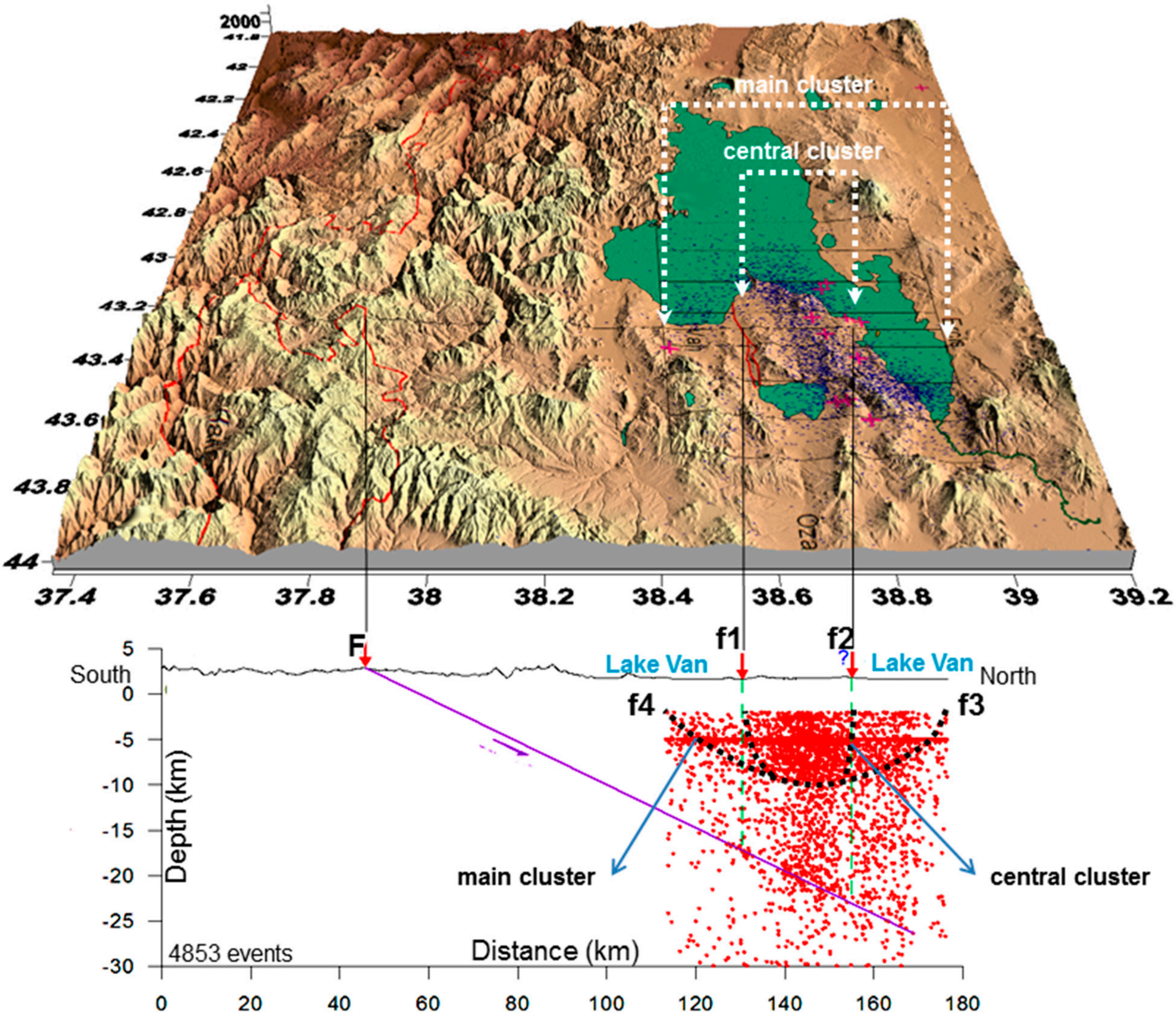
main cluster
central cluster
F
f1
f2
f3
f4
Lake Van
Lake Van
South
North
Depth (km)
Distance (km)
4853 events
main cluster
central cluster

Fig. 6

doi:10.20944/preprints201806.0466.v1

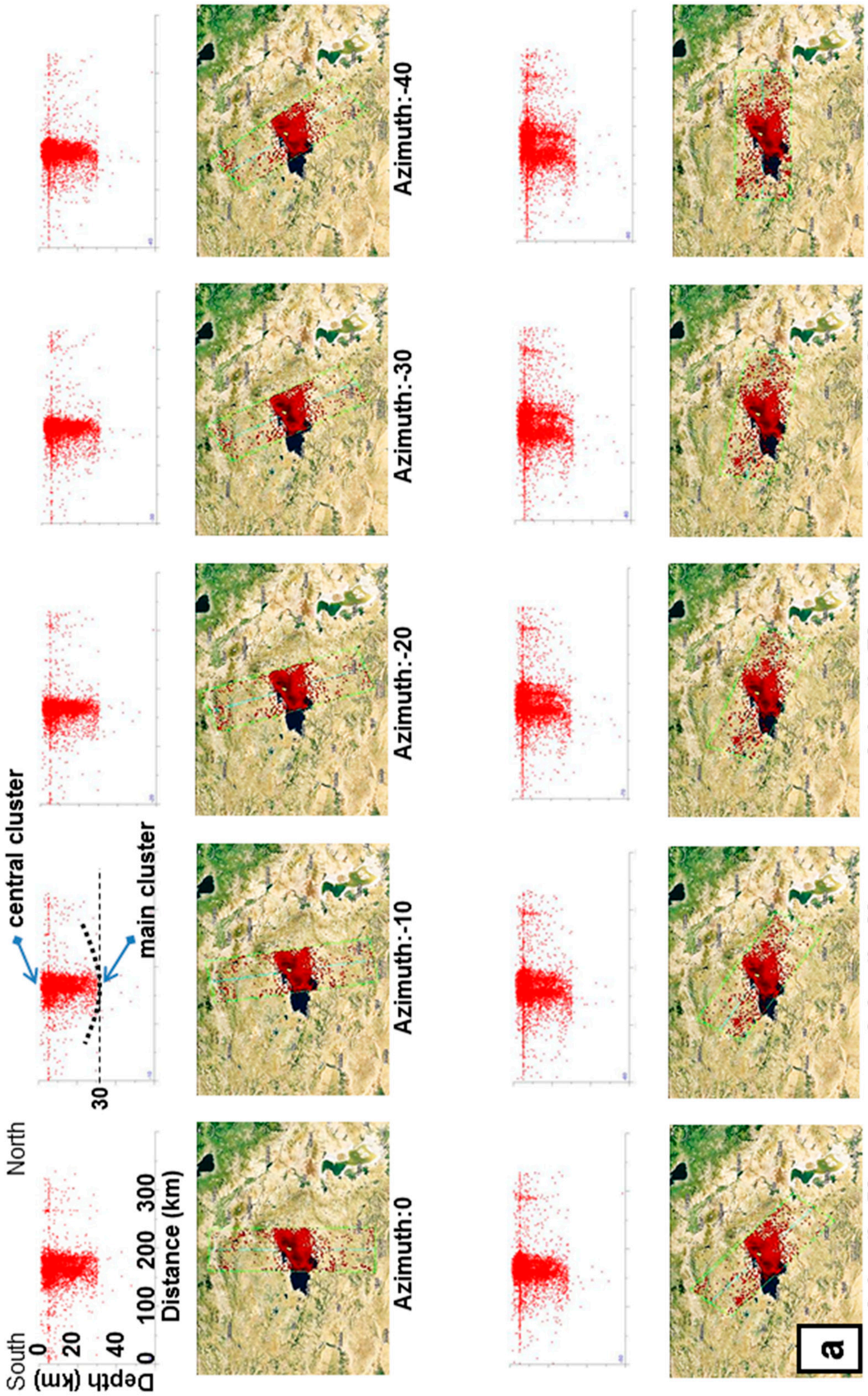

Fig. 7a

 doi:10.20944/preprints201806.0466.v1

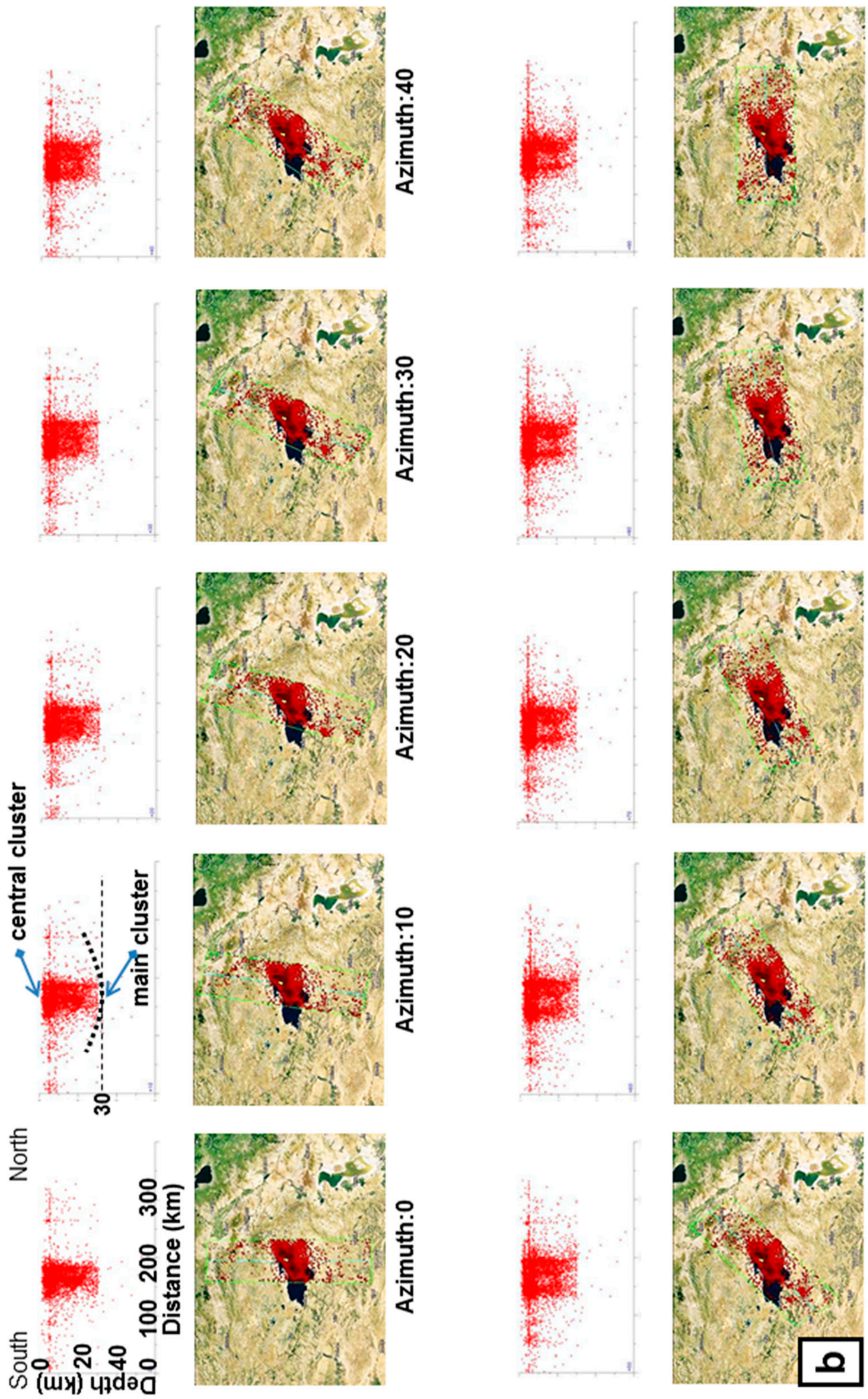

Fig. 7b

Preprints (www.preprints.org) | NOT PEER-REVIEWED | Posted: 28 June 2018 doi:10.20944/preprints201806.0466.v1

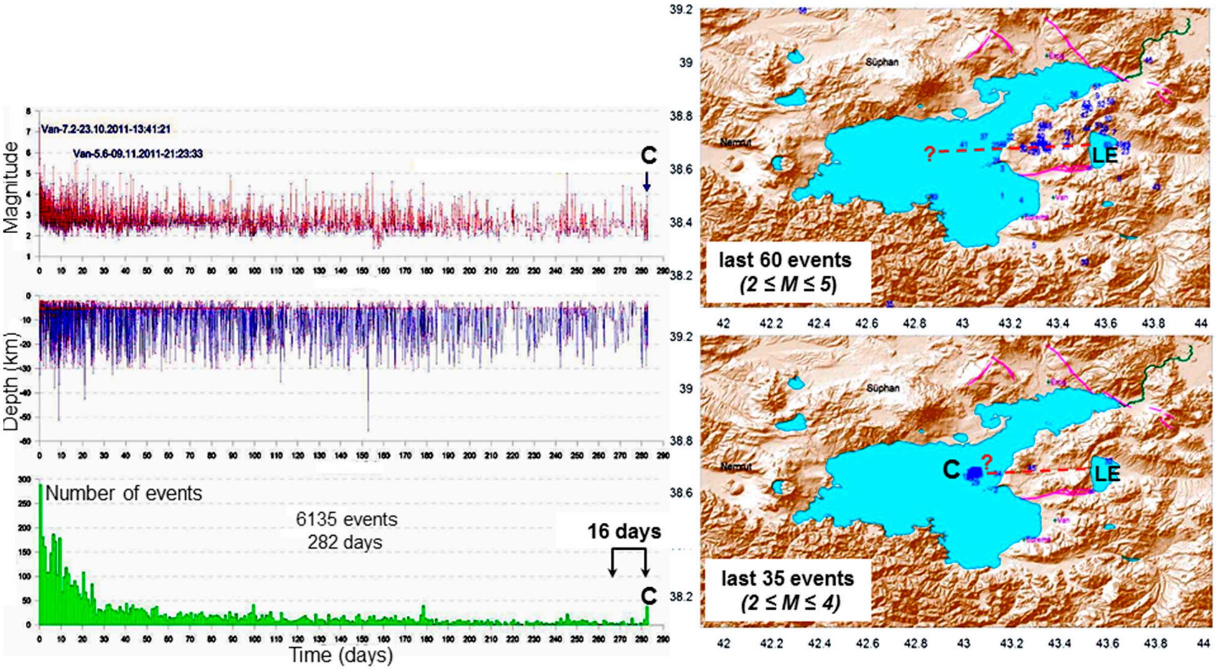

Fig. 8

Preprints (www.preprints.org) | NOT PEER-REVIEWED | Posted: 28 June 2018 doi:10.20944/preprints201806.0466.v1

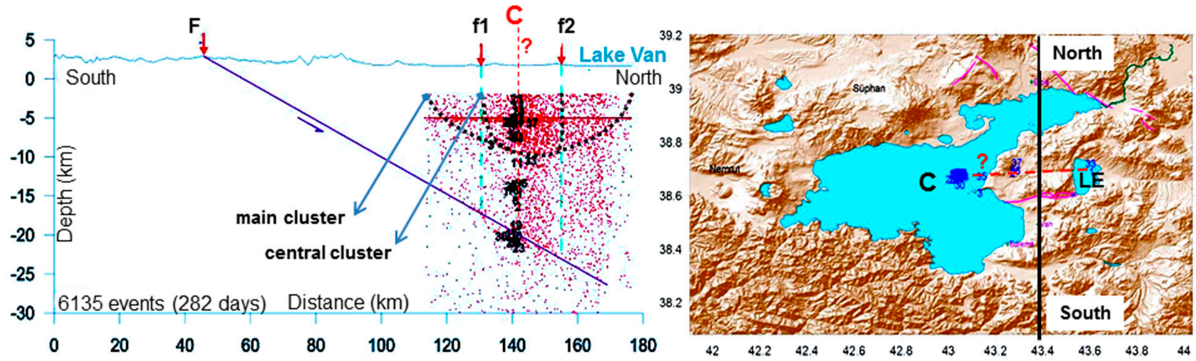

Fig. 9

doi:10.20944/preprints201806.0466.v1

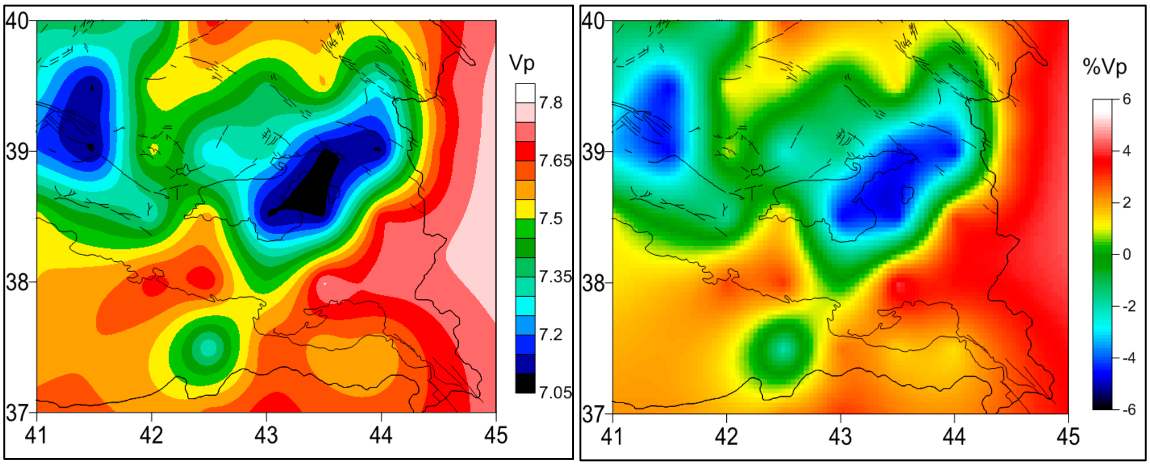

Fig. A1

Preprints (www.preprints.org) | NOT PEER-REVIEWED | Posted: 28 June 2018
doi:10.20944/preprints201806.0466.v1

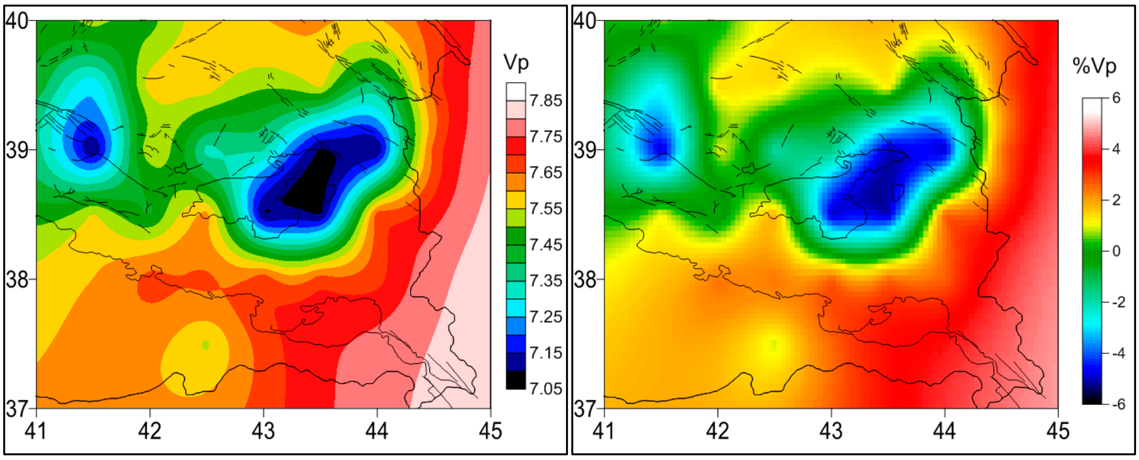

Fig. A2

Preprints (www.preprints.org) | NOT PEER-REVIEWED | Posted: 28 June 2018 doi:10.20944/preprints201806.0466.v1

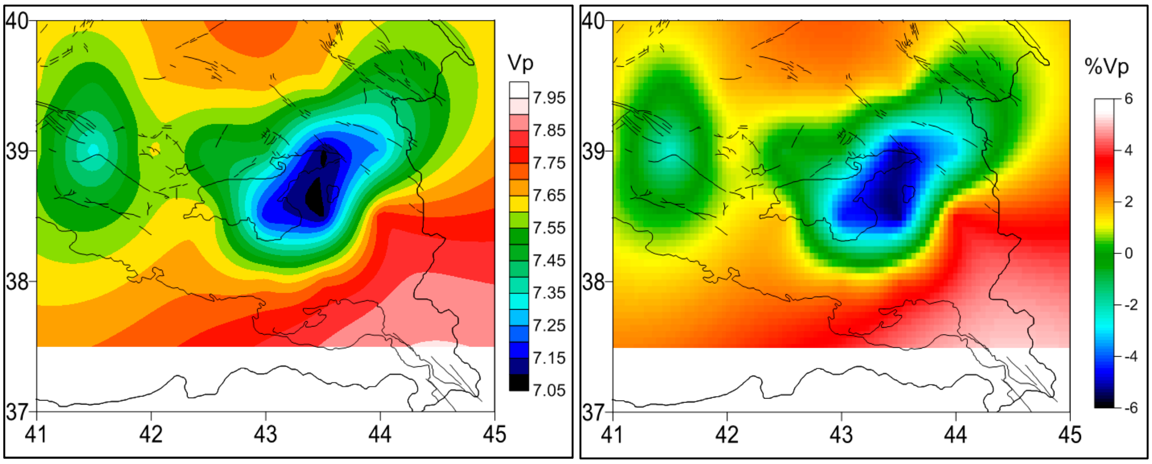

Fig. A3

Preprints (www.preprints.org) | NOT PEER-REVIEWED | Posted: 28 June 2018 doi:10.20944/preprints201806.0466.v1

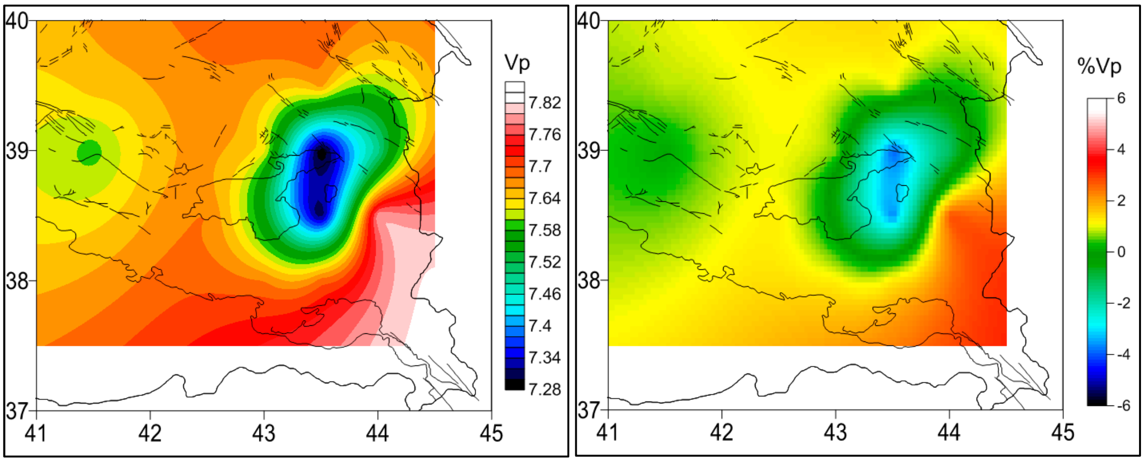

Fig. A4

Preprints (www.preprints.org) | NOT PEER-REVIEWED | Posted: 28 June 2018 doi:10.20944/preprints201806.0466.v1

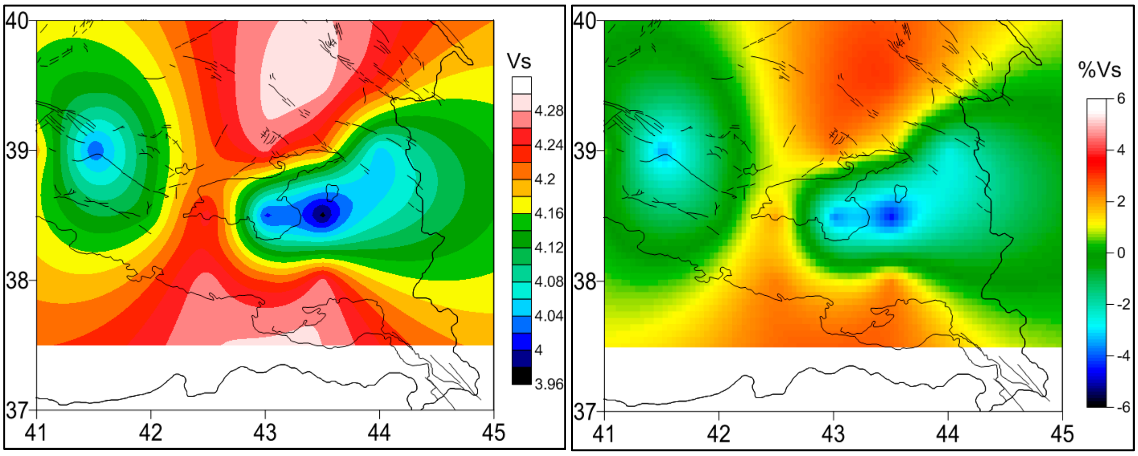

Fig. A5

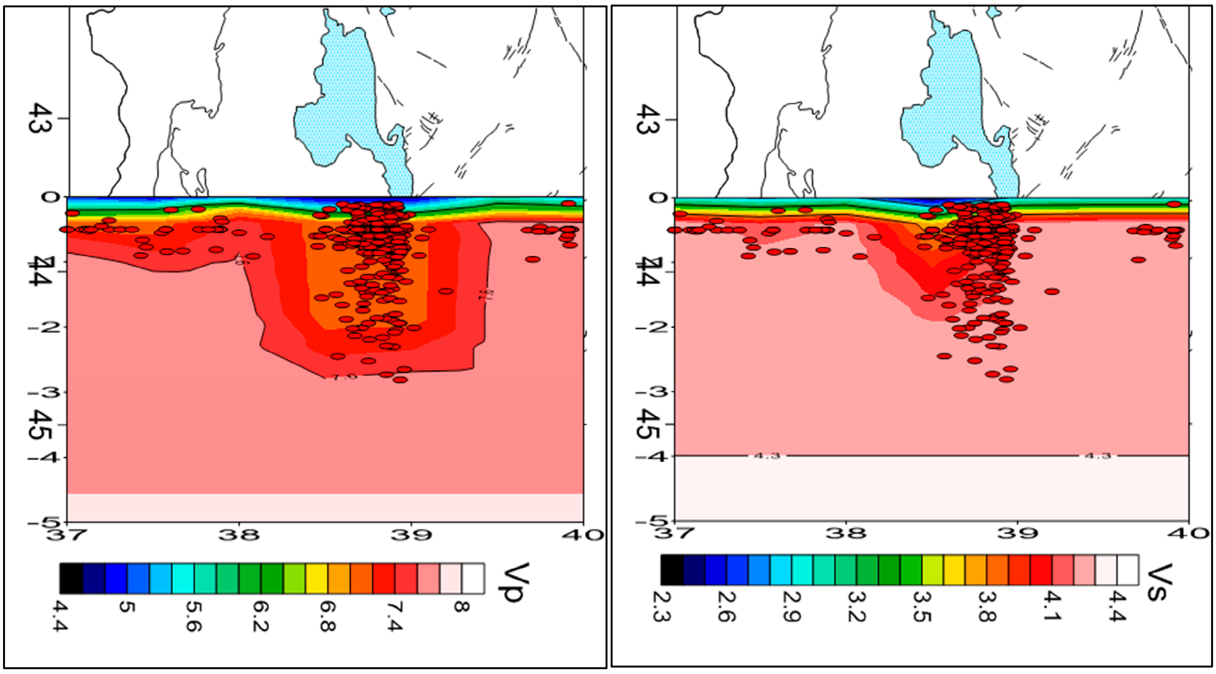
Vp
37
38
39
40
43
44
45
0
-1
-2
-3
-4
-5
4.4
5
5.6
6.2
6.8
7.4
8
Vs
2.3
2.6
2.9
3.2
3.5
3.8
4.1
4.4

Fig. B1

Preprints (www.preprints.org) | NOT PEER-REVIEWED | Posted: 28 June 2018 doi:10.20944/preprints201806.0466.v1

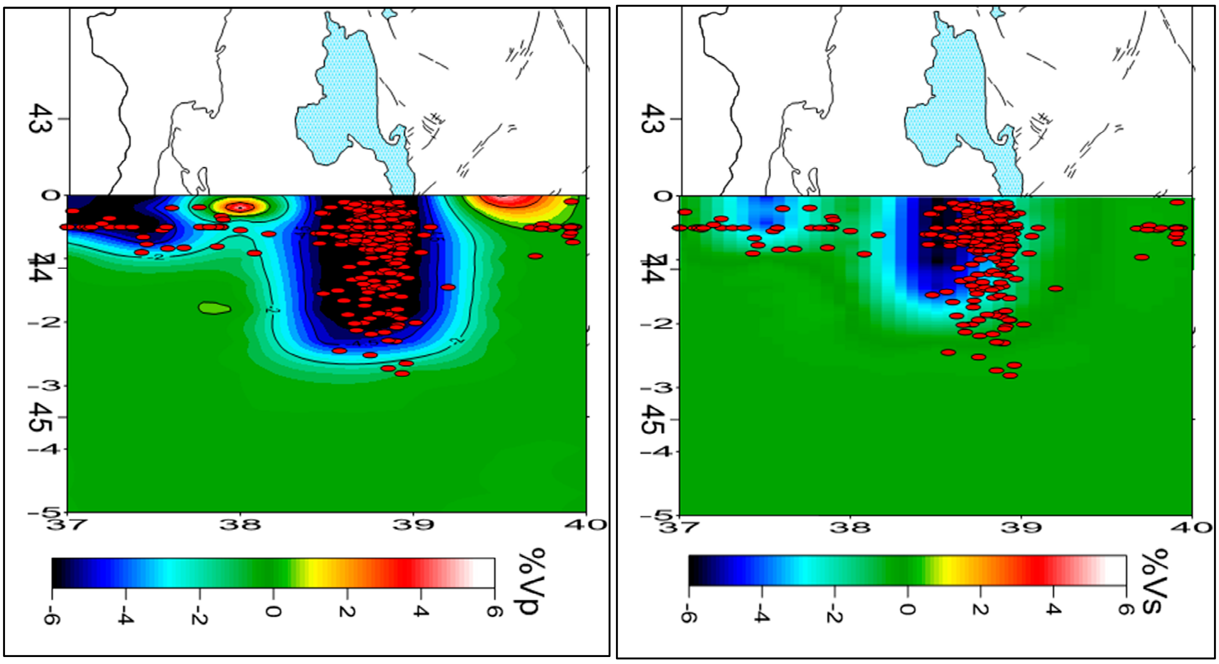

Fig. B2